

## RESEARCH

### **Pre- to post-Cordilleran transposition history of Joss Mountain: Insights into the exhumation of the Shuswap complex, southeastern Canadian Cordillera**

Davide Zanoni<sup>1,\*</sup>, Yvette D. Kuiper<sup>2</sup>, and Paul F. Williams<sup>3</sup>

<sup>1</sup> DIPARTIMENTO DI SCIENZE DELLA TERRA “A. DESIO,” UNIVERSITÀ DEGLI STUDI DI MILANO, VIA MANGIAGALLI 34, 20133 MILANO, ITALY \*davide.zanoni@unimi.it

<sup>2</sup> DEPARTMENT OF GEOLOGY AND GEOLOGICAL ENGINEERING, COLORADO SCHOOL OF MINES, 1516 ILLINOIS STREET, GOLDEN, COLORADO 80401, USA

<sup>3</sup> DEPARTMENT OF EARTH SCIENCES, UNIVERSITY OF NEW BRUNSWICK, 2 BAILEY DRIVE, FREDERICTON, NEW BRUNSWICK, E3B 5A3, CANADA

## ABSTRACT

We present new multiscale structural, mineral chemical, and U-Pb isotope dilution–thermal ionization mass spectrometry (ID-TIMS) data in order to unravel part of the tectono-metamorphic evolution of the Shuswap complex in the southern Canadian Cordillera. We reconstructed the pressure-temperature-deformation-time (P-T-d-t) history of the Joss Mountain domain within the Shuswap complex. The west-dipping Greenbush shear zone separates the Joss Mountain domain from the structurally lower Thor-Odin culmination to the east, the southern culmination of the Monashee complex, and one of the structurally deepest parts of the Shuswap complex. At Joss Mountain, the protolith of an orthogneiss crystallized at ca. 360 Ma which is consistent with Late Devonian arc magmatism along the western paleomargin of North America. Joss Mountain metasedimentary rocks and orthogneiss were transposed at ~21–29 km depth over a period of at least 20 m.y., and possibly more than 38 m.y., during Late Cretaceous to Paleocene mature stages of Cordilleran continental collision. This mature collision took place while slow detachment of the subducted oceanic lithosphere occurred and thermal conditions were approaching those of a crust undergoing postorogenic thermal relaxation. Transposition at Joss Mountain ended earlier and exhumation started earlier than in the Monashee complex. Exhumation occurred under conditions of near-isothermal decompression and geothermal gradients consistent with lithospheric thinning. Earlier and slower exhumation of the Joss Mountain domain than of the adjacent northwestern Thor-Odin culmination may have resulted from normal movement along the Greenbush shear zone contributing to the exhumation of the Shuswap complex.

## INTRODUCTION

This work contributes to the reconstruction of the tectono-metamorphic evolution of middle- to lower-crustal units during the North American Cordilleran orogeny by providing insight into vertical movements of tectonic slices and variations in geothermal regime with time. Our focus is the tectono-metamorphic

history of the Joss Mountain domain (see Williams and Jiang, 2005) within the Shuswap complex of the southeastern Canadian Cordillera. We constructed the pressure-temperature-deformation-time (P-T-d-t) path of the Joss Mountain domain based on new multiscale structural and metamorphic data integrated with new and existing U-Pb isotope dilution–thermal ionization mass spectrometry (ID-TIMS).

We then compared the P-T-d-t path of the Joss Mountain domain with that of the northwestern Thor-Odin culmination (Spalla et al., 2011; Fig. 1) in order to interpret a comprehensive tectono-metamorphic history of part of the Shuswap complex.

Our working approach relies on the reconstruction as far back as possible of the complete structural and metamorphic history in rocks of various compositions. This approach enables us to detect relict structural domains and mineral assemblages and has proven to be crucial for the recognition of different tectono-metamorphic units hidden within homogeneous lithostratigraphic associations, or in domains overprinted by a dominant metamorphic imprint (e.g., Spalla and Gosso, 1999). The formation of a dominant metamorphic imprint, which is characterized by the mineral assemblage defining the dominant fabric, depends on susceptibility of rocks to deformation and metamorphism. Because of strain partitioning and bulk rock composition, the geologic memory of polymetamorphic tectonites is heterogeneous (e.g., Myers, 1970; Mørk, 1985), and different structures (i.e., coronite, tectonite, and mylonite; Lardeaux and Spalla, 1990) can be coeval and defined by the same (if the rock volume is compositionally homogeneous) or compatible (if the rock volume is compositionally heterogeneous) metamorphic assemblages (e.g., Lardeaux and Spalla, 1991; Spalla et al., 2000; Gosso et al., 2010; Zanoni et al., 2010, and references therein). In this study, metamorphic conditions during formation of consecutive structures throughout the deformation history of Joss Mountain rocks were reconstructed based on thermobarometric estimates of structure-related equilibrium mineral assemblages (cf. Spalla et al., 2005; Hobbs et al., 2010; Rebay et al., 2012, and references therein) in schists.

## GEOLOGICAL SETTING

The Canadian Cordillera (inset of Fig. 1) has been divided into five belts, which are distinguished by lithostratigraphic association and tectonic style (Monger et al., 1982). The Foreland belt consists of a fold-and-thrust belt involving Precambrian to Mesozoic sedimentary sequences that unconformably overlie North American crystalline basement (Price and Mountjoy, 1970; Gabrielse et al., 1991). The Intermontane and Insular belts (inset of Fig. 1) represent groups of allochthonous terranes that were mostly accreted during the Triassic through Late Cretaceous (Monger et al., 1994; Murphy et al., 1995; Gehrels et al., 2009; Beranek and Mortensen, 2011). The Coast belt (inset of Fig. 1) is a plutonic complex that lies on the boundary between the Intermontane and Insular superterrane (Monger et al., 1982). The Omineca belt is a polydeformed metamorphic and igneous belt that separates the foreland from the hinterland. In southeastern British Columbia, it includes exposures of igneous and metamorphic rocks of the Precambrian North American craton, overlain by Paleoproterozoic to early Paleozoic metasedimentary sequences (e.g., Monger et al., 1982; Scammell and Brown, 1990; Armstrong et al., 1991; Gabrielse et al., 1991; Crowley, 1997, 1999). These rocks were deformed and exhumed as a consequence of Middle Jurassic to Eocene Cordilleran tectonism (e.g., Monger et al., 1982; Kuiper et al., 2006; Kruse and Williams, 2007; Gibson et al., 2008) related to accretion of allochthonous terranes (e.g., Monger et al., 1982; Gibson et al., 2008; Simony and Carr, 2011), a ribbon continent (Johnston, 2008; Hildebrand, 2009; Kent and Irving, 2010), or volcanic archipelagos (Sigloch and Mihalynuk, 2013, and references therein) to the western paleomargin of the North American craton (Laurentia).

Within the southern Omineca belt, the Shuswap metamorphic complex lies in the footwall of the Eocene Okanagan Valley–Eagle River and Columbia River normal fault systems (Read and Brown, 1981; Parrish et al., 1988; Brown and Carr, 1990; Carr, 1995; Johnson and Brown, 1996; Johnson, 2006; Brown et al., 2012; Fig. 1). The Monashee complex (Fig. 1) exposes some of the structurally deepest rocks of the Shuswap complex (e.g., Brown and Read, 1983) similar to the Malton, Valhalla, Grand Fork, and Priest River complexes (e.g., Wanless and Reesor, 1975; Simony and Carr, 1997; Digel et al., 1998; Doughty et al., 1998; Schaub et al., 2002; Laberge and Pattison, 2007; Cubley and Pattison, 2012). The Monashee complex consists of two structural culminations: Frenchman Cap and Thor-Odin. The cores of these culminations mostly consist of Paleoproterozoic high-grade polymetamorphic migmatitic paragneiss and orthogneiss, which are part of the Precambrian North American craton (Wanless and Reesor, 1975; Armstrong et al., 1991; Parkinson, 1991). The cores are overlain by a Paleoproterozoic to early Paleozoic (Kuiper et al., 2014) metasedimentary cover consisting of quartzite, pelitic schist, semipelitic schist, marble, calc-silicate gneiss, and quartzo-feldspathic gneiss (Brown, 1980; Read, 1980; Journeay and Brown, 1986; Scammell and Brown, 1990; Armstrong et al., 1991; Parrish, 1995; Johnston et al., 2000; Spark, 2001; Kruse et al., 2004). A quartzite or feldspathic quartzite at the base of the metasedimentary cover is interpreted to unconformably overlie basement gneiss (Fyles, 1970; Journeay, 1986; Ross and Parrish, 1991).

At least one other quartzite layer exists within the metasedimentary cover, which has a zircon provenance signature distinct from the basal quartzite and is potentially much younger (Kuiper et al., 2014). Within the Shuswap complex, the Joss Mountain domain (Fig. 2) structurally overlies the Monashee complex. This domain consists of Neoproterozoic or younger metasedimentary rocks and orthogneiss (Johnson, 1994; Parrish, 1995, and references therein), and it is considered part of the Selkirk allochthon (e.g., Johnston et al., 2000; Gervais, 2009). This domain is separated from the Thor-Odin culmination by the westerly dipping normal-sense Greenbush shear zone (Johnston et al., 2000; Kruse and Williams, 2007). Rocks of the Joss Mountain domain are similar to those of the Monashee metasedimentary cover in the northwestern Thor-Odin culmination, but they contain more metagranitoid, calc-silicate gneiss, and marble (Journeay, 1986; Johnston et al., 2000).

**Structural Geology of the Thor-Odin Culmination** In Thor-Odin, core and cover rocks are transposed in response to a top-to-the-northeast, noncoaxial flow. At least two generations of tight to isoclinal folds (F1 and F2) are intrafolial to the transposition foliation (ST). They verge between northeast and north. More open folds (F3) that fold ST are considered part of the last increments of the transposition deformation flow, because they display the same northeast vergence as the overall transposition flow (Johnston et al., 2000; Williams and Jiang, 2005; Kuiper et al., 2006). In view of the progression of deformation that produced ST, the intrafolial folds are referred to as mature and the more open folds as immature (Williams and Jiang, 2005), and the deformation is referred to as DT (Spalla et al., 2011). DT structures are overprinted by north-trending upright folds (F4 of Johnston et al., 2000; Williams and Jiang, 2005; DT+1 of Spalla et al., 2011).

Along the west side of Thor-Odin, the transition between rocks of the Monashee complex and those of the overlying Joss Mountain domain is marked by a zone of down-to-the-west shear bands known as the Greenbush shear zone, which is located within rocks of the Monashee complex (Johnston et al., 2000; Kruse and Williams, 2007). ST steepens in this zone, and a lineation associated with ST swings from a general south to southwest orientation to a more westerly orientation. The zone is interpreted as the product of Eocene crustal extension (D5 of Johnston et al., 2000; or DT+2 of Spalla et al., 2011), and it is overprinted by Eocene brittle strike-slip and normal faults (Kruse and Williams, 2005, 2007). At the latitude of our study area, the Greenbush shear zone spatially coincides with the Monashee décollement (Read and Brown,

1981; Brodie and Rutter, 1985; Journeay and Brown, 1986; Brown et al., 1992; McNicoll and Brown, 1995; Gervais et al., 2010), a top-to-the-northeast reverse shear zone that is interpreted to no longer exist in the region between Joss Mountain and the Thor-Odin culmination (Johnston et al., 2000; Spark, 2001; Kruse and Williams, 2007; Simony and Carr, 2011). To the south, the continuation of the Greenbush shear zone, the Slate Mountain shear zone (Fig. 1), is mapped within the Thor-Odin culmination and does not coincide with the previously interpreted Monashee décollement (Kruse and Williams, 2007). Eocene subvertical pegmatites (e.g., Johnston et al., 2000) and lamprophyres (e.g., Lane, 1984; Adams et al., 2005) intruded during E–W crustal extension.

**Estimated Metamorphic Conditions for the Thor-Odin Culmination** Various estimates of metamorphic conditions have been obtained in the past 35 yr in different parts of the Thor-Odin culmination (Fig. 3). Temperatures of 620–685 °C at pressures of 0.6–0.7 GPa, obtained from clinopyroxene-garnet–amphibolites at Three Valley Gap (box 2 in Fig. 3; Ghent et al., 1977), were recalculated at 700 °C and 0.61 GPa (Lane et al., 1989). In the same locality, anatectic metapelites yielded 0.75–0.9 GPa and 720–800 °C (box 1 in Fig. 3; Nyman et al., 1995). Temperatures of 725–800 °C and pressures of 0.8–1.0 GPa were estimated from gedrite-cordierite-schists, metapelitic rocks, and amphibolite boudins in central southern Thor-Odin (boxes 3, 4, and 5 in Fig. 3; Norlander et al., 2002). In the southern Thor-Odin culmination, peak conditions between 0.9 and 1.0 GPa and 720 °C and 770 °C were estimated (box 6 in Fig. 3; Goergen and Whitney, 2012).

A comprehensive P–T–d–t history has been described for northwestern Thor-Odin (lines 7 and 8 in Fig. 3; Spalla et al., 2011). Metamorphic conditions were estimated at 700–850 °C and 0.80–1.25 GPa and  $T > 800$  °C and  $P < 0.90$  GPa for the pre-ST stages in kyanite- and spinel-bearing metapelites, respectively. Temperatures between 600 °C and 800 °C and pressures between 0.50 and 1.05 GPa were derived for the syn-ST stage, while post-ST conditions were at 585–680 °C and 0.45–0.60 GPa. In metabasites, 690–820 °C and 0.85–1.25 GPa and 670–760 °C and 0.35–0.80 GPa were estimated for the pre-ST and syn-ST stages, respectively. The post-ST stage occurred at  $P < 0.50$  GPa and  $T < 675$  °C (Fig. 3; Spalla et al., 2011).

#### Ages of Metamorphism

Metamorphic zircon and monazite at Three Valley Gap yielded  $71.7 \pm 1.5$  Ma and  $57.5 \pm 5.0$  Ma ID-TIMS ages, respectively (cf. Parkinson, 1992; Gilley, 1999; Kuiper, 2003). Based on U–Pb ID-TIMS and sensitive high-resolution ion microprobe (SHRIMP) monazite and zircon analyses, ages of peak of metamorphism in the Thor-Odin culmination have been interpreted between ca. 65 Ma at high structural levels and ca. 51 Ma at low structural levels (Parrish et al., 1988; Coleman, 1990; Johnston et al., 2000; Hinchey et al., 2006). A Ky-bearing pegmatite in an F1/F2 boudin neck in the metasedimentary cover of Blanket Mountain is dated at  $54.5 \pm 1$  Ma, and F3 folds are crosscut by a  $51.0 \pm 0.5$  Ma pegmatite and  $50.2 \pm 0.5$  Ma tourmaline-bearing aplites and pegmatites (Johnston et al., 2000). Lamprophyre dikes consistently intersect the youngest undeformed pegmatite dikes, and, based on the  $^{40}\text{Ar}/^{39}\text{Ar}$  age of contact-metamorphic muscovite in the host rock of a lamprophyre at Three Valley Gap, they are considered to be  $48.4 \pm 0.3$  Ma in age (Adams et al., 2005).

Monazite, zircon, titanite, and xenotime U–Pb ID-TIMS dates in Frenchman Cap, interpreted as ages of metamorphism, range from  $77.7 \pm 0.3$  Ma at the highest structural levels (Gibson et al., 1999) to ca. 49 Ma at the deepest structural levels of the complex (Crowley and Parrish, 1999). Ages of deformation and metamorphism as old as ca. 170 Ma have been reported within the structurally highest levels of the Selkirk allochthon, in the Selkirk, Monashee, and Cariboo Mountains (Gibson et al., 2005), and are supported by age constraints based on stratigraphy and the fossil record (Parrish, 1995, and references therein). All

together, the data were interpreted as indicating a younging of structures and peak thermal metamorphism toward deeper structural levels in the Selkirk allochthon and Monashee complex (e.g., Johnson, 1994; Parrish, 1995; Crowley and Parrish, 1999; Johnston, 1998; Gibson et al., 1999, 2005, 2008).

## ROCK TYPES AND MESOSCOPIC STRUCTURES AT JOSS MOUNTAIN

The Joss Mountain rock assemblage is dominated by marble, calc-silicate gneiss, and layers of granitic and granodioritic orthogneiss. Orthogneiss forms two 50–150-m-thick sheets, and some thinner lenses and layers, above the upper sheet, in the metasedimentary rocks of the Joss Mountain assemblage. Marble units contain boudinaged diopside-rich layers. Layers of metapelitic schist, within both calc-silicate gneiss and orthogneiss, are less common and, at the 1:35,000 scale, reach mappable thicknesses only in the western Joss Mountain area (Fig. 2), where they are mainly in contact with marble. Quartzite is rare and only thick enough to be mapped in the western part of the area (Fig. 2).

The main structural feature of the area is a composite transposition foliation (ST), which affects all rock types (Fig. 4A), with the exception of the youngest pegmatite and lamprophyre dikes. The basement cover units of the Thor-Odin culmination and the rocks of the Joss Mountain domain are all strongly transposed, and the boundaries between them are diffuse and marked by alternations of the adjacent units (Johnston et al., 2000; Kruse and Williams, 2007; Spalla et al., 2011). Within ST, at least two generations of mature intrafolial folds (F1 and F2) are preserved (Fig. 4B) and are interpreted as having developed during transposition. ST dips generally shallowly toward the west, F1 and F2 hinge lines generally plunge shallowly southwesterly, parallel to the transport direction, and immature (open to tight) F3 folds that fold ST plunge northwesterly (Johnston, 1998; Johnston et al., 2000). Whereas in the northwestern Thor-Odin culmination, F1, F2, and F3 folds all verge to the northeast (e.g., Johnston et al., 2000; Williams and Jiang, 2005, and references therein), in the Joss Mountain domain, F1 and F2 folds verge to the northeast, and F3 folds verge to the southwest (Johnston et al., 2000). The reversal in vergence has previously been explained in terms of ductile extrusion and/or channel flow during transposition (Johnston et al., 2000; Williams and Jiang, 2005; Kuiper et al., 2006), where F3 folds represent the latest increments of the overall transposition.

Ages of metamorphism young downward, from the Joss Mountain domain toward the core of the Thor-Odin culmination. Within the Joss Mountain domain, a  $93.0 \pm 1.5$  Ma U-Pb ID-TIMS monazite age in metapelitic schist has been interpreted as the age of ST development (Johnston et al., 2000). A  $73.4 \pm 1.5$  Ma leucogranite dike that intersects ST and is folded by F3 constrains the age of F3 development, and thus the last increments of ST, to younger than  $73.4 \pm 1.5$  Ma (Johnston et al., 2000). Gentle to open, gently north-plunging upright F4 folds overprint F3 folds (Johnston et al., 2000). Up to 4-m-thick E-W-trending white pegmatite dikes intersect ST (Figs. 4C and 4D) and F3. Lamprophyre dikes, showing chilled margins, crosscut all ductile structures and also postdate all pegmatite dikes at Joss Mountain.

## MICROSTRUCTURES

Microstructures as outlined by Zwart (1962), Hobbs et al. (1976), Vernon (2004), and Passchier and Trouw (2005) are described to define mineral assemblages on the grounds of relationships between mineral growth and deformation. In the following descriptions mineral abbreviations from Whitney and Evans (2010) are used with the exception of white mica (Wm). Schist samples have been chosen to constrain P-T conditions of consecutive stages of fabric development and therefore are used to constrain quantitative P-T-d-t paths. The types of schist are separated into Wm- and Bt-bearing groups, where ST is defined in the latter by Bt only, and in the former by Wm plus Bt. These two groups of schist contain the most suitable mineral assemblages for obtaining thermobarometric estimates of the Joss Mountain rocks. In addition, we

describe microstructural features of orthogneiss and folded and crosscutting felsic intrusive rocks, which, in part, were used for U-Pb ID-TIMS geochronology.

The transposition foliation (ST) is the dominant fabric in all analyzed rocks, except in the crosscutting pegmatite dikes. Relict pre-ST metamorphic assemblages are mainly preserved in the cores of Grt porphyroblasts, whereas post-STa and post-STb mineral assemblages define older and younger post-ST microscale shears or coronitic structures. Throughout this section, roman numerals are used to identify the generations of mineral growth for each individual mineral. These roman numerals do not necessarily equate to a specific generation of metamorphism. Roman numerals are not used where a mineral phase grew only in one single metamorphic assemblage (e.g., Sil).

In Wm-bearing schist, ST is characterized by films defined by shape and lattice preferred orientation (SPO and LPO, respectively) of WmII and BtII, minor SPO of IlmII, and lithons of Qz, PlII, and minor KfsII. Locally, phyllosilicates and quartz-feldspar form centimeter-thick ST-parallel layers. WmI, BtI, and minor KfsI form coarse-grained relict porphyroclasts wrapped by ST (Figs. 5A and 5B). Intrafolial folds, preserved between ST films, are defined by plastically deformed WmI and BtI or by Qz-bearing layers (Fig. 5C), indicating that these minerals predate at least part of ST development. The cores of Grt porphyroblasts contain a pre-ST mineral assemblage that includes BtI, Qz, PlI, and WmI, which form euhedral crystals with rational grain boundaries (inset of Fig. 5D). Coarse-grained Grt porphyroblasts show rare inclusion trails oblique to ST. These trails, defined also by BtI, PlI, WmI, IlmI, and Qz, are straight in the core and curved in the rim of the porphyroblasts, and they are locally continuous with ST in the rock matrix; these features suggest multiple growth stages for the coarse-grained Grt, with the core (GrtI) predating ST and the rim (GrtII) growing during ST development.

Alternatively, this microstructure may indicate that strain rate was initially low relative to the growth rate of Grt porphyroblasts. Inclusions are more abundant in the cores than in the syn-ST rims of the garnet porphyroblasts (Fig. 5D). Fine-grained GrtII grains occur in the micaceous films and show rational grain boundaries with BtII and WmII. They are locally elongate, with their long axis parallel to ST (Fig. 5E). Post-STa microscales are defined by BtIII  $\pm$  Sil. Locally, they contain Wm porphyroclasts as mica-fish structures. Fine-grained Sil crystals overgrew WmI porphyroclasts (inset of Fig. 5A) and formed, with minor BtIII, reaction rims between WmII and GrtII (Fig. 5F). Locally, Sil formed prismatic laths along WmII [001] cleavages or replaced Wm grains, in a more pervasive manner, where lattice deformation, such as kinking, occurred. Where the replacement of previous mineral phases is (nearly) complete, Sil forms lens-shaped microdomains of prismatic or fibrolitic crystals that may replace Grt porphyroblasts. The domains that mimic ST possibly formed at the expense of micaceous layers richer in pelitic components than the norm. Sil does not occur in samples from the northern part of the study area (e.g., samples 13 and 52; Fig. 2). Rare greenish BtIV and ChI occur in the fractures of Grt porphyroblasts. ChI and WmIII partially replaced BtIII and Sil that define post-STa microscales.

ChI and KfsIII grew at the expense of Bt (Fig. 5G), and KfsIII is rimmed by rare Ab. Post-STb microscales contain abundant ChI, KfsIII, WmIII, Ab, and minor Rt and Fe-oxides (Fig. 5H). Rare Tur forms euhedral crystals overprinting ST. These microstructural features allow definition of the relative chronology of the following equilibrium mineral assemblages in Wm-bearing schist:

pre-ST: Qz, BtI, WmI, PlI, GrtI, IlmI,  $\pm$  KfsI,

syn-ST: Qz, BtII, WmII, PlII, GrtII, IlmII,  $\pm$  KfsII,

post-STa: Qz, BtIII, ± Sil,

post-STb: Qz, Chl, WmIII, KfsIII, ± Ab, ± Rt, ± Fe-oxides, ± Tur, ± BtIV.

In Bt-bearing schist, ST is defined by BtII films, formed by crystals with a good ST-parallel LPO and SPO and PIII and Qz layers with minor KfsII. Locally, ST is a well-spaced foliation with quartz-feldspar lenses up to a few millimeters thick. PIII shows deformation and minor growth twins. Rare relict KfsI and PII are deformed and wrapped by ST. Grt porphyroblasts are characterized by an internal foliation defined by IlmI that in the core is at a high angle and in the outer part is bent into parallelism with the external ST (Fig. 6A), suggesting that the cores of the porphyroblasts may be interpreted as pre-ST (GrtI) and the outer part as syn-ST (GrtII). Where the inclusion trail foliation is only slightly deflected into a sigmoidal shape and is continuous with the external ST, GrtII porphyroblasts are considered synkinematic with ST (Fig. 6B). Where Grt forms up to centimeter-sized porphyroblasts, the inclusion trail is defined also by Qz and minor PII and BtI, in addition to IlmI (Fig. 6C).

Locally, centimeter-sized Grt porphyroblasts are skeletal. Rare Ep and Ttn grains are visible in backscattered electron (BSE) images only. Ep occurs within ST strain shadows of Grt porphyroblasts, and Ttn forms crystals parallel to ST. PIII and minor Qz form thick (up to ~0.5 mm) coronas around Grt porphyroblasts, and in these microsites, PIII grains show a lower internal deformation than PIII and Qz grains defining ST (Fig. 6D), based on more frequent undulose extinction and deformation twinning in PIII than in PIII and more growth twinning in PIII than PIII. PIII also exists as thin rims between BtII and Grt porphyroblasts (Fig. 6E). BtII laths are parallel to the axial surface of F3 microfolds and can be interpreted as defining an incipient foliation (Fig. 6F). Since F3 folds are grouped within the syntransposition structures, the Bt grains parallel to F3 axial surfaces are labeled BtII3. Locally, randomly oriented BtIII grains occupy coronas rimming Grt porphyroblasts. Where ST displays a C-C' or C-S fabric, BtIII may also define the microscales that are inclined at a small angle to ST. Chl is rare and partially replaces Bt or fills fractures intersecting Grt porphyroblasts, which are normally approximately orthogonal to the inclusion trail foliation. In summary, the following mineral assemblages exist in Bt-bearing schist:

pre-ST: Qz, PII, BtI, GrtI, ± KfsI, ± IlmI,

syn-ST: Qz, PIII, BtII, GrtII, ± KfsII, ± IlmII, ± Ep, ± Ttn,

post-STa: Qz, PIII, BtIII,

post-STb: ± Chl.

Orthogneiss consists of Fsp, Qz, and Bt, with minor Grt. Zrn is an accessory phase. The pervasive foliation, which is the same as the ST transposition foliation in schist types, is defined by Qz-rich and Bt-Fsp-rich millimeter-scale layers, with rare Grt. Qz forms elongate crystals parallel to ST. Within single crystals, subgrain boundaries are parallel and at a high angle to ST (Fig. 7A). Bt laths show LPO and SPO parallel to ST (Fig. 7A). Within Fsp-rich layers, Pl and Kfs form granoblastic structures and show growth twinning and minor deformation twinning; polysynthetic twins of Pl are both parallel and at a high angle to ST (Fig. 7B). Also, Kfs and Pl form elongate crystals parallel to ST. Fine-grained Wm grew at the expense of Kfs and locally forms aggregates that mimic the twin boundary of Pl grains. Zrn forms euhedral crystals (Fig. 7B). Chl grew mimetically at the expense of Bt, locally completely replacing Bt.

Crosscutting pegmatite contains subhedral Fsp and Qz, minor Wm and Grt, accessory Zrn, Mnz, Ttn, and Ilm, and retrograde Ep and fine-grained Wm. Fsp occurs as Pl and Kfs phenocrysts. Pl phenocrysts show

polysynthetic growth twinning and rare myrmekites against Kfs crystal edges (Fig. 7C). These myrmekites are interpreted as consistent with slight granular deformation assisted by fluid circulation (e.g., Menegon et al., 2006). Kfs shows indented grain boundaries and faint flame perthites (Fig. 7D); the latter are interpreted as a result of a slight solid-state deformation under greenschist-facies conditions (e.g., Pryer and Robin, 1996). Wm is recrystallized along its edges. Qz, Fsp, and Wm show slight undulose extinction. Taken together, these microstructural features are consistent with a weak postmagmatic crystallization deformation.

## MINERAL CHEMISTRY

### Methods

Mineral compositions were determined using a Jeol JXA-8200 electron microprobe (WDS [wavelength dispersive X-ray spectroscopy], accelerating voltage of 15 kV, beam current of 15 nA) and a Jeol JSM-6400 scanning electron microscope (SEM; EDS [energy dispersive X-ray spectroscopy], accelerating voltage of 15 kV, beam current of 1.5 nA) operating in the Earth Sciences Department of Milano University and Microscopy and Microanalysis Facility of the University of New Brunswick, respectively. Natural silicates were used as standards, and the results were corrected for matrix effects using a conventional ZAF (corrections for atomic number effects, absorption, and fluorescence) procedure. Mineral proportional formulae were calculated using JPT java program (Zucali, 2005), on the basis of 22 oxygen atoms for biotite and white mica, 12 oxygen atoms for garnet, 8 oxygen atoms for feldspar, and 28 oxygen atoms for chlorite. Fe<sup>3+</sup> was recalculated only for garnet as described in Droop (1987). We describe the composition variations of mineral phases with respect to their relative timing of crystallization during consecutive deformation stages in Wm- and Bt-bearing schist. In the following paragraphs, the composition of each mineral phase is described for the two types of schist. The full mineral phase name is reported at the beginning of the description of each phase composition; afterwards only mineral abbreviations are used.

### Results

The three generations of white mica (Wm) have a constant composition; WmIII has the lowest Ti values, and the average XMg ratio (Green and Usdansky, 1986) increases slightly from 0.80 to 0.82 for WmI to WmIII (Fig. 8A; Table 1). Within single samples, WmII shows XPg (sample 8; WmI = 0.08; WmII = 0.09–0.10; WmIII = 0.09) and XMg (sample 55; WmI = 0.41–0.53; WmII = 0.54–0.66; WmIII = 0.38–0.53) ratios slightly higher than WmI and WmIII. WmIII grains, growing in Grt fractures or between Grt and Bt, show a lower XMg ratio (0.38–0.39) than grains defining post-STb shears (XMg = 0.46–0.58).

Biotite (Bt; Fig. 8B), in both Wm- and Bt-bearing schist, shows a composition mainly in the field of Fe<sup>2+</sup>-biotite (see Guidotti et al., 1975). In Wm-bearing schist, BtI has the highest average content in Ti and is lower in AlVI than any other generation of Bt. This different composition is because, being mostly preserved in the core of Grt porphyroblasts, BtI would be less re-equilibrated with the rock matrix (Fig. 8B; Table 1). However, BtIII grains that grew with Sil at the expenses of Wm reach the highest Ti content of all Bt generations (Table 1), whereas BtIII that grew in symplectites around Grt shows locally the lowest Ti content. Among BtII grains, those preserved in fine-grained GrtII show the highest Ti values, whereas the lowest Ti values are usually in BtII grains in contact with a GrtII rim. The XMg ratio is similar for BtI, BtII, and BtIII. Bt in Bt-bearing schist is poorer in AlVI and shows a higher average XMg ratio than Bt in Wm-bearing schist. In these rocks, the different Bt generations show less variation than Bt in Wm-bearing schist (Table 1). The Ti content and XMg ratio are constant, whereas AlVI increases from BtI to BtIII (Table 1). The highest Ti content occurs in BtI grains included in Grt porphyroblasts or in deformed grains within ST. BtII grains

with lower Ti content are in contact with the rim of Grt porphyroblasts. BtIII grains defining the post-STa shears show higher Ti content than BtIII grains rimming Grt porphyroblasts with PlIII. Grains from all Bt generations in Wm-bearing schist show a dispersion toward low Ti contents (Fig. 8B), and this may be due to a reequilibration postdating the post-STa stage that seems to have not affected Bt-bearing schist. Bt grains showing Ti depletion were not considered for estimating temperature (see following).

Garnet (Grt) compositions are dominated by the almandine molecule, which varies between 0.69 and 0.79, and 0.60 and 0.67 in Wm- and Bt-bearing schist, respectively (Fig. 9A). The grossular content is higher in Grt from Bt-bearing schist (0.13–0.21) than in Grt from Wm-bearing schist (0.01–0.06). The latter is relatively enriched in pyrope (0.10–0.15) versus Grt in Bt-bearing schist (0.05–0.12). Spessartine shows similar concentrations in Grt from both rock types (Bt-schists = 0.04–0.13; Wm-schists = 0.05–0.13). The andradite component in Grt from both Wm and Bt-bearing schist is mostly zero, but, where present, is up to 0.03. In Wm-bearing schist, GrtI and GrtII show similar composition, with a slight decrease in Ca from GrtI to GrtII (Table 1; Fig. 9A). The composite GrtI/II porphyroblasts show an increase in Fe<sup>2+</sup> and a decrease in Ca (Fig. 9B) from core to rim. Centimeter-sized composite GrtI/II porphyroblasts in Bt-bearing schist show a pronounced compositional zoning (open black and dark-gray squares in Fig. 9) characterized by an increase in Fe<sup>2+</sup> and Mg and a decrease in Ca and Mn from the core (GrtI) to the rim (GrtII) (Table 1; Fig. 9A). This marked zoning may be due to a better preservation of the core of large porphyroblasts by solid state diffusion, which affects Grt at temperatures higher than 600 °C (Yardley, 1977; Caddick et al., 2010).

Plagioclase (Pl) in Wm-bearing schist is relatively enriched in Ab compared to the Bt-bearing schist (Table 1; Fig. 10A). In Wm-bearing schist, PlI is oligoclase and may have up to andesinic composition, whereas PlII is oligoclase, and PlIII is albite. The most remarkable composition difference between PlI (An = 31%–32%) and PlII (An = 25%–27%) occurs in sample 42. In Bt-bearing schist PlI, PlII, and PlIII are andesine and can reach a labradoritic composition, in PlI (Table 1). K-feldspar (Kfs) analyzed in post-STb assemblages and in syn-ST assemblages in Wm- and Bt-bearing schist is orthoclase (Fig. 10A).

Chlorite (Chl; Fig. 10B) is ripidolite and pycnochlorite in Wm-bearing schist and aphrosiderite and brunsvigite (Hey, 1954) in Bt-bearing schist. In Wm-bearing schist, Chl in Grt fractures shows the highest Al content. The XMg ratio is higher in Chl grains marking the post-STb shears and lower in Chl grains replacing Bt. Al and XMg are lower in Chl in Bt-bearing schist than in Wm-bearing schist.

## U-Pb ID-TIMS GEOCHRONOLOGY

### Methods

We dated a sample of transposed orthogneiss and a pegmatite crosscutting F3 folds to constrain the ages of the transposition and F3 development, respectively. U-Pb geochronology was carried out over a decade ago at Carleton University. While methods have improved in the past decade, leading to more precise data, reducing the error on our data would not change our interpreted tectono-metamorphic history. Heavy minerals were separated from ~10–25 kg rock samples by standard crushing, grinding, Rogers Gold™ table separation, and heavy liquid separation. Mineral separates containing the least magnetic zircon and monazite were separated by Frantz™ magnetic separation techniques. BSE images of selected grains, not used for geochronology, were taken at Carleton University. Minerals with the fewest inclusions and fractures, the best clarity, and no visible cores and overgrowths were selected for dating by handpicking under an optical microscope. Where zircon tips were used, these were either cut by hand, or tips broken during crushing and grinding were selected. All zircon fractions were air abraded with pyrite (Krogh, 1982), and washed in warm HNO<sub>3</sub> to remove abrasion residues. Minerals selected for dating were spiked with a

mixed  $^{205}\text{Pb}$ - $^{233}\text{U}$ - $^{235}\text{U}$  tracer (Parrish and Krogh, 1987) and dissolved in HF (zircon) or HCl (monazite) in Teflon<sup>TM</sup> microcapsules (Parrish, 1987). U and Pb were separated using anion exchange column chemistry procedures as described by Parrish et al. (1987; cf. Krogh, 1973; Roddick et al., 1987), and their isotopic compositions were measured on a Finnigan-MAT261 variable multicollector mass spectrometer (Roddick et al., 1987). Procedural blanks were generally less than 5 pg for U and 6–60 pg for Pb. Common-Pb corrections were made using Pb compositions derived from Stacey and Kramers (1975). Decay constants recommended by Steiger and Jäger (1977) were used. Errors in isotope ratios were estimated using numerical error propagation (Roddick, 1987). All errors for ages are reported at the 2s level. Discordia chords through data were calculated using a modified York (1968) regression (Parrish et al., 1987). Data were plotted using Isoplot/Ex v. 2.49 (Ludwig, 2001).

### Joss Mountain Orthogneiss

Sample 123 of Joss Mountain orthogneiss is from the upper sheet (Fig. 2), which outcrops over the Joss Mountain alpine area. It consists of a medium-grained, gray, homogeneous, Bt-bearing leucocratic metagranitoid and contains Fsp, Qz, and Bt, with minor subhedral Grt crystals, accessory Zrn, and retrograde Ser, Wm, and Chl. This sample has a SSW-dipping gneissosity/foliation, interpreted as ST, and a weak shallowly plunging, E-W-trending Bt lineation. Four single zircon crystals and two multiple tip fractions, E and K, were dated to constrain the protolith age of the Joss Mountain orthogneiss (Fig. 11A; Table 2). BSE images show concentric zonation, and in some crystals thin overgrowths, but no inherited cores (Fig. 11A). Based on morphology and concentric zonation, the crystals are interpreted as having an igneous origin. The protolith age of the Joss Mountain orthogneiss is  $362 \pm 13$  Ma, based on the weighted average of  $^{207}\text{Pb}/^{206}\text{Pb}$  ages of fractions B, C, E, I, J, and K (Table 2).

### Joss Mountain Pegmatite

Sample 4 is from an ~4-m-wide E-W-trending vertical granitic pegmatite dike that can be traced for 150 m along strike (Figs. 2 and 4C). This pegmatite does not display a chilled margin and crosscuts ST (Fig. 4D), SW-verging F3 folds, and the boundary between metapelitic schist and orthogneiss. Sample 4 contains subhedral Fsp, Qz, Wm, and Grt, accessory Zrn, Mnz, Ttn, and Ilm, and retrograde Ep and Ser. Slight crystal-plastic deformation affects Qz, Fsp, and Wm. Since the pegmatite cuts F3 folds, this granular-scale deformation postdates F3 folds and may be coeval with F4. Three zircon fractions and five single monazite grains were analyzed (Fig. 11B; Table 2). Based on euhedral crystal shapes, igneous (concentric and sector) zonation in BSE images (Fig. 11B), and the absence of cores, the monazite crystals appear to have an igneous origin. Some crystals have thin overgrowths. The dated crystals were all pale yellow with excellent clarity. Fraction M2 is subrounded and has an indentation. All others are euhedral. Two monazite growth ages can be distinguished. Fractions M1–M4 are reversely discordant, whereas M5 is normally discordant, probably due to an older inherited component. The weighted average  $^{207}\text{Pb}/^{235}\text{U}$  age from fractions M2, M3, and M4 is  $69.2 \pm 1.6$  Ma. The  $^{207}\text{Pb}/^{235}\text{U}$  age of M1 is  $55.4 \pm 0.6$  Ma. Zircon fraction A consists of eight tips, B of one tip, and D of 15 small clear zircons. BSE images of zircon crystals show strong alteration and metamictization, presumably as a result of high U (Fig. 11B, grain 1), which is common in pegmatite. All zircon fractions yielded discordant data, which can be explained by inheritance, overgrowth, Pb loss, or a combination. However, the error ellipses of fractions A and B overlap with the concordia curve at ca. 69 Ma, supporting the  $69.2 \pm 1.6$  Ma monazite age. The Th/U ratios of fractions A and B are 0.025 and 0.048, respectively, which is significantly higher than the <0.01 ratios for metamorphic zircon in the Thor-Odin dome (e.g., Kuiper, 2003; Hinchey et al., 2006).

The U concentrations of these zircon fractions is in the 4000–6000 ppm range, consistent with those for other Cretaceous–Paleocene igneous zircons from felsic intrusives elsewhere in the Monashee complex (e.g., Gibson, 2003; Crowley et al., 2001; Th/U ratios not reported). Thus, the metamict nature, Th/U ratios, and U concentrations of the zircon suggest an igneous origin. The crystallization age of the pegmatite is interpreted as  $69.2 \pm 1.6$  Ma, based on the weighted average  $^{207}\text{Pb}/^{235}\text{U}$  age of monazites M2, M3, and M4, the predominantly euhedral shape of the monazites, and the clustering zircon fractions A and B around that age. Alternatively, the  $55.4 \pm 0.6$  Ma age of M1 could be interpreted as the crystallization age of the pegmatite, which would be supported by the euhedral shape of that monazite (Fig. 11). However, it is unlikely that the ca. 69 Ma population of monazite (and zircon) is inherited, as there are no known intrusive rocks of that age in the area. A paragneiss at Three Valley Gap (Fig. 1) has ca. 71.5 Ma monazite and discordant zircon fractions that plot near slightly older ages along the concordia curve (Kuiper, 2003). However, monazite crystals from that paragneiss display a rounded morphology and sample 123 zircon grains patchy zoning, and its zircon crystals are clear and generally euhedral, and therefore they are not a likely source for the monazite and zircon grains in our pegmatite. For these reasons, we interpret the crystallization age of the pegmatite as  $69.2 \pm 1.6$  Ma, although a  $55.4 \pm 0.6$  Ma crystallization age cannot be ruled out. A felsic dike at Joss Mountain, folded by F3, is  $73.4 \pm 1.5$  Ma in age (Johnston et al., 2000). The felsic dike contains the F3 axial-planar foliation. We use the ages of the crosscutting pegmatite and folded felsic dike, observed at two different outcrops, to constrain the age of F3 at Joss Mountain between ca. 73 Ma and ca. 69 Ma and possibly between ca. 73 Ma and ca. 55 Ma. If the former is true, then the  $55.4 \pm 0.6$  Ma single monazite age in the crosscutting pegmatite may reflect a later (metamorphic?) event. If the latter is correct, then the ca. 69 Ma monazite is inherited.

## P-T-d-t EVOLUTION

### Methods

P-T estimates were obtained for each deformational and metamorphic stage, using mineral assemblages, differentiated on the basis of microstructural analysis, and the chemical composition of their mineral phases, in order to constrain the P-T-d-t path of the Joss Mountain schist. To constrain the pre-ST conditions, the compositions of mineral grains preserved in the cores of Grt porphyroblasts were used. To constrain the syn-ST conditions, grains defining ST and the rims of Grt porphyroblasts were used. For both post-STa and post-STb conditions, the compositions of grains defining the related microscopic shears and coronitic structures were used. P-T conditions were estimated using independent and well-calibrated geothermometers and geobarometers (see Table 3 caption). The THERMOCALC software (Holland and Powell, 1998) was used to derive univariant equilibrium reaction curves between end members, for which the activity was calculated using the AX program (Holland and Powell, 1998), and for P-T estimates by the average P-T calculation method (Powell and Holland, 1994). Finally, we also referred to experimental or calculated reaction curves from the literature (Fig. 12).

### Results

Pre-ST and syn-ST assemblages yield similar P-T conditions in both Wm- and Bt-bearing schist, with Bt-bearing schist recording these two stages at higher temperatures and pressures than Wm-bearing schist. Pre-ST and syn-ST conditions mostly plot in the high-temperature amphibolitefacies field (Ernst and Liou, 2008). In Wm-bearing schist, the pre- to syn-ST path is retrograde, with the exception of one sample, which yielded an indication of a prograde path (sample 42). For the prograde relict assemblage, pre-ST conditions are estimated between 0.50 and 0.56 GPa and 610 °C and 650 °C (Table 3). At lower pressures and higher temperatures, this P-T field is limited by the calculated univariant reaction curve  $\text{Grt} + \text{Wm} = \text{Bt} + \text{Sil} + \text{Qz}$  at

~0.5 GPa and 650 °C (Fig. 12). Along the retrograde path, pre-ST temperatures are estimated between ~615 °C and 700 °C and pressure between 0.56 and 0.73 GPa (Fig. 12; Table 3). Syn-ST conditions are estimated at temperatures between 610 °C and 700 °C and pressures between ~0.53 and 0.72 GPa and are consistent with the univariant curves  $Ms + Ab + Qz = Kfs + Als + L$  (Le Breton and Thompson, 1988) and  $Kfs + Ms + Bt + H_2O = Grt + L$  (White et al., 2001), which limit this P-T field toward higher temperature, and  $Grt + Wm = Bt + Sil + Qz$ , which limits the P-T field toward lower pressures (Fig. 12). The geothermometer by Kleemann and Reinhardt (1994) was not applied to sample 52 because the Mn content in Grt is higher than that recommended. The temperatures from the geothermometer by Ganguly and Saxena (1984), which yielded values higher than the curves leading to the breakdown of Wm,  $Ms + Ab + Qz = Kfs + Als + L$  (Le Breton and Thompson, 1988) and  $Kfs + Ms + Bt + H_2O = Grt + L$  (White et al., 2001), were not considered reliable. Post-STa conditions are characterized by temperatures between 600 °C and 700 °C (Table 3) and pressures between 0.25 and 0.6 GPa. On average, these temperatures are lower than temperatures for the reaction  $Ms + Ab + Qz = Kfs + Als + L$  (Le Breton and Thompson, 1988), and the maximum values are lower than the reaction curve  $Kfs + Ms + Bt + H_2O = Grt + L$  (White et al., 2001). The lowest and highest pressures are constrained by the  $Sil = And$  and  $Grt + Wm = Bt + Sil + Qz$  reaction curves, respectively. The reaction  $Bt + Als = Grt + Crd$  (Spear and Cheney, 1989) constrains the low-pressure limits of this field at values higher than 0.2 GPa. Post-STb conditions are lower than 420 °C based on the calculated reaction  $Chl + Kfs = Bt + Qz + H_2O$  and higher than 270 °C based on the composition of Chl (Table 3).

Bt-bearing schist records a retrograde path from the pre-ST to the syn-ST stage. Pre-ST pressures are estimated between 0.82 and 0.96 GPa, and temperatures are estimated between 610 °C and 730 °C, whereas syn-ST pressures are estimated between 0.74 and 0.92 GPa and temperatures between ~640 °C and 750 °C (Fig. 12; Table 3). The geothermometers based on the Fe-Mg exchange reaction between Grt and Bt by Perchuk et al. (1985), Kaneko and Miyano (2004), and Kleemann and Reinhardt (1994) were not applied to these rocks because Ca content in Grt is higher than that recommended. Post-STa temperatures are estimated between 620 °C and 700 °C (Fig. 12; Table 3).

In summary, mineral phases constituting pre- and syn-ST equilibrium assemblages show similar compositions, perhaps due to the post-STa reequilibration, which may have partially reset the composition of previous mineral phases. If true, estimated pressures for pre- and syn-ST stages would be minimum pressures, since post-STa assemblages developed under lower pressures than pre- and syn-ST assemblages. Thus, similar P-T conditions for pre- and syn-ST assemblages result, and the difference is even smaller for the retrograde path. This little difference may suggest that the pre-ST fabrics were reworked during the development of ST or represent an earlier increment of transposition itself. Since pre- and syn-ST conditions, yielding the retrograde path, are similar also where Grt zoning is pronounced, this difference in P-T conditions may be primary, and pre-ST may actually represent an earlier transposition (syn-ST) increment. Thus, the pre-ST assemblage indicating a possible prograde path may be the only pre-ST relict. Higher temperatures and pressures for pre- and syn-ST stages in Bt-bearing schist than in Wm-bearing schist perhaps result from the different bulk rock composition, as suggested by the different composition of mineral phases and the occurrence of Wm and Sil only in Wm-bearing schist. The different bulk composition may control the P-T conditions at which phases can react to form mineral assemblages, and, in this case, the Bt-bearing schist may have recorded transposition at different P-T conditions than Wm-bearing schist. Grt from Bt-bearing schist is relatively depleted in Fe compared with Grt in Wm-bearing schist (Fig. 9A); pressures and temperatures estimated from Grt-bearing assemblages in the two schist types are consistent with the increase of Fe/(Fe + Mg) ratio of isopleths with decreases of pressure and temperature (e.g., Spear et al., 1999). Phase composition suggests that the bulk chemistry of Bt-bearing

schist is richer in Ca than that of Wm-bearing schist, indicating that minimum pressure for transposition could be estimated from the latter.

Pressures and temperatures estimated by applying the average P-T calculation method (Powell and Holland, 1994) partly result in larger ranges and higher values than those obtained by classical thermobarometers, which are most consistent with the experimental reaction curves. On the other hand, the comparison of different thermobarometric methods has shown that the average P-T calculation method overestimates temperature (e.g., Gulbin, 2012).

## DISCUSSION

### P-T-d Constraints from Wm- and Bt-Bearing Schist of the Joss Mountain Domain

Multiscale structural analysis of Wm- and Bt-bearing schist at Joss Mountain shows that the mineral assemblages that were stable during the development of the regional ST transposition foliation are Qz, BtII, WmII, PlII, GrtII, IlmII, ± KfsII in Wm-bearing schist and Qz, PlII, BtII, GrtII, ± KfsII, ± IlmII, ± Ep, ± Ttn in Bt-bearing schist. P-T estimates on these assemblages indicate that ST developed at 0.53–0.72 GPa and 610–700 °C in Wm-bearing schist and at 0.74–0.92 GPa and 640–750 °C in Bt-bearing schist (Fig. 12). Pre-ST assemblages developed at 0.56–0.73 GPa and 615–700 °C in Wm-bearing schist and at 0.82–0.96 GPa and 610–730 °C in Bt-bearing schist. Pre-ST assemblages, preserved in core of Grt porphyroblasts, formed at slightly higher pressures and temperatures than those under which syn-ST assemblages marking the matrix foliation developed (Fig. 12). In one sample (42) of Wm-bearing schist, the pre-ST relict assemblage yields pressures (0.50–0.56 GPa) and temperatures (610–650 °C) lower than that of syn-ST assemblages. The similar P-T conditions of pre- and syn-ST assemblages yielding the retrograde path suggest that the retrograde path results from a continuous transposition, where assemblages in the Grt core recorded earlier transposition stages than assemblages marking the matrix foliation. Thus, the pre-ST assemblage suggesting a prograde path in Wm-bearing schist (sample 42) can be interpreted as the only pretransposition relict. The stronger variation of Ca content between PlI and PlII in sample 42 than in other samples may be responsible for the bigger differences in pressures along the prograde than retrograde path (Fig. 12; Table 3), which may have resulted from partial preservation of pre-ST compositions through subsequent reworking.

Post-STa developed fabrics under temperatures between 600 °C and 700 °C and pressures between 0.25 and 0.60 GPa as a consequence of a near-isothermal decompression. The microscales developed during post-STa may be related to the upright F4 folding, as the F4-related (DT+1) shear zones developed under high temperature and low pressure in the northwestern Thor-Odin culmination (Spalla et al., 2011). The post-STb mineral assemblages crystallized during the final cooling under greenschist-facies conditions (Fig. 12).

The average P/T ratio estimated for the conditions of ST development in the Joss Mountain schist is between  $\sim 0.95 \times 10^{-3} \text{ GPa } ^\circ\text{C}^{-1}$  and  $\sim 1.18 \times 10^{-3} \text{ GPa } ^\circ\text{C}^{-1}$ , and up to  $\sim 1.30 \times 10^{-3} \text{ GPa } ^\circ\text{C}^{-1}$ , considering the retrograde pre-ST as part of transposition (Table 4). The syn-ST P/T ratios estimated for ST at Joss Mountain are higher than 0.63 and 0.84  $\text{GPa } ^\circ\text{C}^{-1}$ , estimated for the ST development in the metapelite of the northwestern Thor-Odin culmination (Spalla et al., 2011). Even lower P/T ratios of  $\sim 0.65 \times 10^{-3} \text{ GPa } ^\circ\text{C}^{-1}$  characterize the post-STa stage at Joss Mountain (Table 4). The variation of the P/T ratio with time shows that the overall P-T path recorded by Joss Mountain schist represents a decompressional evolution characterized by an increase of the geothermal gradient. A similar exhumation path but at slightly higher temperature (Fig. 13A) was reconstructed for the northwestern Thor-Odin culmination (Spalla et al., 2011).

During the decompression path of the Joss Mountain domain, the Bt-bearing schist may have recorded earlier increments of transposition, at higher pressures and temperatures, than Wm-bearing schist. This is consistent with (1) the general decompression path as preserved by the sequence of assemblages from the core of Grt porphyroblasts toward assemblages marking the matrix ST, and (2) higher syn-ST thermal gradients recorded by Wm- than by Bt-bearing schist (Table 4). Based on these points, the assemblage yielding a prograde path in Wm-bearing schist is interpreted as predating the earliest transposition increment recorded by Bt-bearing schist.

Lower temperatures during exhumation of the Joss Mountain domain with respect to the exhumation of the northwestern Thor-Odin culmination are consistent with the different relative abundance of Wm versus Sil in these two domains. At Joss Mountain, Wm forms abundant and fresh crystals defining ST and porphyroclasts in Wm-bearing schist, whereas in northwestern Thor-Odin, scarce Wm grains grew during late-greenschistfacies re-equilibration, at the expense of syn-ST minerals that include Sil (Spalla et al., 2011). Furthermore, in the northwestern Thor-Odin culmination, Sil is abundant in pelitic rocks and marks the transposition foliation (ST), while at Joss Mountain, less abundant Sil developed during the post- STa stage, in coronitic textures or in localized microshears. This microstructural and petrographic evidence is consistent with ST having developed at temperatures on average lower than 700 °C, under which Wm is stable, at Joss Mountain (see White et al., 2001; Fig. 12), and with ST temperatures up to ~800 °C and approaching that of Bt dehydration melting (Le Breton and Thompson, 1988) in the northwestern Thor-Odin culmination. Using an average density for the continental crust of 2.9 g/cm<sup>3</sup> (Spear, 1993) and the average pressures estimated for ST development in Wm- and Bt-bearing schist, ST development at Joss Mountain is estimated to have occurred on average at a depth between 21 and 29 km (Table 4). In the same way, from the average pressures estimated for ST development in metapelitic schist of the northwestern Thor-Odin culmination (Spalla et al., 2011), average depths between 22 and 30 km are estimated for the development of ST. Thus, ST developed at similar depths in the Joss Mountain domain and in the northwestern Thor-Odin culmination, but temperatures during exhumation of the Joss Mountain domain were lower than in the northwestern Thor-Odin culmination (Fig. 13A).

#### Age Constraints on Transposition at Joss Mountain

The ca. 360 Ma U-Pb zircon age of the Joss Mountain orthogneiss records the emplacement or crystallization age of the orthogneiss protolith, which is consistent with the age of widespread Late Devonian to early Mississippian igneous activity that occurred in the Kootenay terrane (Reesor and Moore, 1971; Okulitch et al., 1975; Okulitch, 1985; Parrish, 1992; Johnson, 1994), an ancestral pericratonic North American parautochthonous terrane (e.g., Paradis et al., 2006; Colpron et al., 2007, and references therein). In particular, the Joss Mountain orthogneiss protolith may be related to the evolution of a continental arc on the western margin of Laurentia, the remnants of which are part of the Eagle Bay assemblage of the Kootenay terrane (e.g., Paradis et al., 2006; Nelson et al., 2013, and references therein). The orthogneiss protolith age confirms that at Joss Mountain, the Cordilleran transposition (ST development) is younger than 360 Ma, consistent with transposition occurring in response to convergence, regardless of whether that occurred by terrane accretion beginning in the Middle Jurassic (e.g., Carr, 1992; Parrish, 1995; Crowley and Parrish, 1999; Gibson et al., 1999, 2008; Crowley et al., 2001), or by the convergence of a ribbon continent (i.e., Stikinia-Wrangellia) between the Late Triassic and Early Cretaceous, and subsequent dextral transpressional collision during the Late Cretaceous to Eocene (e.g., Kent and Irving, 2010, and references therein). A  $93 \pm 1.5$  Ma monazite age from a metapelitic schist from Joss Mountain is interpreted as representing the peak of metamorphism (Johnston et al., 2000) during transposition. F3 folding at Joss Mountain can be interpreted as having occurred between ca. 73 Ma and ca.

69 Ma and possibly between ca. 73 Ma and ca. 55 Ma (see earlier herein). In any case, F3 occurred after the peak of metamorphism. Since F3 folding is interpreted as having developed late during syn-Cordilleran transposition, transposition lasted at least 20 m.y., and possibly longer than 38 m.y. at Joss Mountain. A long-lived ST history justifies the wide range of P-T conditions yielded by Bt- and Wm-bearing schist for transposition development. Similarly, in the northwestern Thor-Odin culmination, transposition was long-lived and occurred under a broad range of P-T conditions (Spalla et al., 2011). However, F3 folding in the northwestern Thor-Odin culmination was younger than at Joss Mountain, between ca. 54.5 Ma and ca. 51 Ma, based on monazite ages in deformed and crosscutting pegmatites, respectively (Johnston et al., 2000). Thus, transposition in the northwestern Thor-Odin culmination was ongoing at ca. 54.5 Ma and possibly continued until ca. 51 Ma. In the Frenchman Cap culmination, F2 is interpreted as having ceased by 55 Ma at high, and by 49 Ma at low structural levels, based on the ages of deformed and crosscutting felsic intrusives (Crowley et al., 2001; Gervais et al., 2010), indicating that transposition in the Frenchman Cap culmination outlasted transposition in the northwestern Thor-Odin culmination. Our data indicate that transposition in the Joss Mountain domain is older than in the two culminations.

### P-T-d-t Path and Orogenic Evolution

In Figures 13B, 13C, and 13D, the P-T-d path reconstructed for Joss Mountain is compared with the geotherm variation, throughout time and space, calculated by Spalla and Marotta (2007) for a convergent system that evolves from the onset of subduction to postcollisional gravitational collapse. The P-T conditions for the transposition development fit with geotherms calculated for subduction both for the upper and lower plate (Fig. 13B), whereas they fit only with the upper-plate geotherms calculated for continental collision (Fig. 13C). Therefore, the Joss Mountain domain would be better placed on the upper plate during Cordilleran convergence. The metamorphic peak for ST at Joss Mountain is estimated at 93 Ma (Johnston et al., 2000). This time is ~30 m.y. later than the inferred age for the onset of the collision based on various interpretations, including collision of the Rubia ribbon continent at ca. 120 Ma (Hildebrand, 2009), or Angayucham, Mezcalera, and Southern Farallon arcs at ca. 125 Ma (Sigloch and Mihalynuk, 2013), or with the accretion of the Wrangellia terrane in the Cretaceous (Gibson et al., 2008). The ~30 m.y. delay between the onset of collision and the 93 Ma metamorphic peak for ST at Joss Mountain is consistent with predicted times for detachment of the subducted lithospheric slab and therefore with ST being related to a longlasting continental collision. Slab detachment may occur within 8–45 m.y. after the start of the continental collision, depending on lithosphere strength (Marotta et al., 1998; Gerya et al., 2004; Marotta and Spalla, 2007). Because the age of the subducted oceanic plate is ca. 400 Ma, and therefore relatively strong, the detachment of the subducted lithosphere was probably slow (Hildebrand, 2009). Therefore, at Joss Mountain, transposition may reflect a mature stage of continental collision, during which a cold and resistant subducted oceanic lithosphere was necking, and a paleogeotherm was evolving toward the conditions of a thermally relaxed orogenic crust. Since age constraints are lacking, the pre-ST assemblage suggesting a prograde path may have been formed during either subduction or a collisional stage earlier than that of transposition. Both the exhumation paths of the northwestern Thor-Odin culmination (Spalla et al., 2011) and the Joss Mountain domain show tectonic stages developed at low P/T ratios before the final exhumation, which are DT+1 (northwestern Thor-Odin) and post-STa (Joss Mountain), respectively (Fig. 13A). The post-STa stage at Joss Mountain took place during a near-isothermal exhumation, whereas DT+1 in northwestern Thor-Odin was accompanied by an increase in temperature at low-pressure conditions, which led to late partial melting (Spalla et al., 2011), similar to that documented in the southwestern Thor-Odin culmination (Hinckley et al., 2006). The post-STa stage at Joss Mountain records geothermal gradients higher than that of the highest P/T ratio geotherms calculated by Spalla and Marotta (2007) for pure gravitational collapse following continental collision. Within the Shuswap complex,

gravitational collapse was demonstrated previously to be an unsuitable mechanism for the exhumation of the Frenchman Cap culmination (Gervais and Brown, 2011). Our results indicate that the same applies to the thermomechanical evolution of the Joss Mountain domain. Lithospheric thinning may have provided the heat to justify high geothermal gradients, as was suggested for the adjacent northwestern Thor-Odin culmination (Spalla et al., 2011). In the Joss Mountain domain, the transposition history ended after ca. 73 Ma and before 69 Ma and possibly as late as 55.4 Ma, while in the northwestern Thor-Odin culmination, transposition was still ongoing at 54.5 Ma but was over by  $51.0 \pm 0.5$  Ma (cf. Johnston et al., 2000). The age of DT+1 (upright folding) in the northwestern Thor-Odin culmination can be interpreted as younger than  $50.2 \pm 0.5$  Ma, the age of monazite in Tur-bearing pegmatite (sample 9 of Johnston et al., 2000) crosscut by DT+1 shear zones on limbs of DT+1 upright flexural slip folds (Spalla et al., 2011), whereas post-STa fabrics are younger than 55.4 Ma. Thus, transposition at Joss Mountain ended up to ~22 m.y. and possibly as little as 0.9 m.y. earlier than in northwestern Thor-Odin. Therefore, Joss Mountain rocks probably reached shallow crustal levels earlier than rocks in northwestern Thor-Odin. The difference in timing of exhumation between the two domains is also consistent with the general increase of Ap and Zrn fission track ages from Thor-Odin to the rocks structurally above the Greenbush shear zone (Lorenca et al., 2001). Crosscutting lamprophyre dikes at Joss Mountain are probably of the same age as those dated at 48 Ma at Three Valley Gap, as they belong to a widespread regional igneous event (Adams et al., 2005), and exhumation at greenschist-facies conditions probably had ended by that time. By that time, exhumation had also ended in the northwestern Thor-Odin culmination, where the same crosscutting lamprophyre dikes occur (Johnston et al., 2000; Adams et al., 2005; Spalla et al., 2011).

Thus, during the early Eocene, the exhumation rate at Joss Mountain may have been lower than in the northwestern Thor-Odin culmination. Slower and earlier exhumation of the Joss Mountain domain than of the northwestern Thor-Odin culmination is consistent with early Eocene exhumation of the northwestern Thor-Odin culmination due to movement along the normal-sense Greenbush shear zone (cf. Johnston et al., 2000). The normal shearing accommodated by the Greenbush shear zone is consistent and coeval with the normal shearing along other shear zones of the southern Shuswap complex, such as the shallowly west-dipping Okanagan Valley shear zone, bounding the Shuswap complex to the west (Johnson, 2006; Brown et al., 2012), the Granby fault, bounding the western edge of the Grand Fork complex (Laberge and Pattison, 2007; Cuble and Pattison, 2012), and the Valkyr shear zone, bounding the Valhalla complex to the west (Carr et al., 1987; Simony and Carr, 1997). Therefore, the Greenbush shear zone may have played a role in the early Eocene exhumation and unroofing of the Shuswap complex.

Finally, since the P-T-d-t path of the Joss Mountain domain fits best with the geothermal state of the upper plate during convergence (Spalla and Marotta, 2007), and the Shuswap complex is widely considered part of ancestral North America (i.e., Laurentian realm; Nelson et al., 2013), we tentatively interpret a scenario where, during the Cordilleran convergence, oceanic lithosphere subducted beneath the paleo-North America. This may also be consistent with the Three Valley Gap lamprophyre suite occurring in the ancestral North America terrane and interpreted as deriving from a mantle wedge previously contaminated by subduction (Adams et al., 2005), which could have been placed above an eastward-dipping oceanic lithosphere. This interpretation is in contrast with models of westward subduction of oceanic lithosphere of the Laurentian plate beneath the ribbon continent that have been interpreted to lead to Cordilleran collision (Johnston, 2008; Hildebrand, 2009). However, it is consistent with the eastward direction of subduction in the classical interpretation of the accretionary terranes (e.g., Brown et al., 1993; Gibson et al., 2008) and of the Southern Farallon slab (Sigloch and Mihalynuk, 2013).

## CONCLUSIONS

We reconstructed the P-T-d-t history of the Joss Mountain domain in the context of North America Cordilleran orogenesis. The Joss Mountain orthogneiss protolith was emplaced at ca. 360 Ma, when extensive Late Devonian magmatism occurred in the Eagle Bay assemblage of the Kootenay terrane. The orthogneiss protolith may have been related to the development of a magmatic continental arc along the western margin of paleo-North America. Its ca. 360 Ma age constrains the maximum age for transposition at Joss Mountain and is consistent with the age of the beginning of Cordilleran convergence and of Cordilleran orogenesis predicted by accretion of allochthonous terranes and collision of a ribbon continent and volcanic archipelagos. Transposition lasted at least 20 m.y., and possibly more than 38 m.y., and was probably over at 69 Ma, but may have lasted until 55.4 Ma. Transposition developed under average temperatures of 640–700 °C and average depths of 21–29 km. Broad temperature and depth ranges are consistent with the long duration of transposition. The age of transposition and thermal gradients are consistent with transposition during continental collision. Joss Mountain rocks record mature stages of continental collision, when the paleogeotherm was evolving toward one characteristic of thermal relaxation of a crust after orogenic thickening during slow detachment of an old and strong subducted oceanic lithosphere. A possible prograde relict assemblage predating transposition may have resulted from either oceanic subduction or a collisional stage predating transposition. After transposition, initial exhumation transported rocks isothermally to a depth of ~15 km. Exhumation occurred under a geothermal gradient that requires lithospheric thinning. The end of ductile deformation is constrained by 48 Ma lamprophyre dikes, both in northwestern Thor-Odin and at Joss Mountain, making Eocene exhumation rates slower at Joss Mountain than in northern Thor-Odin. These differences in exhumation rates and ages are consistent with normal movement along the Greenbush shear zone, unroofing the northwestern Thor-Odin culmination and contributing to the cumulative exhumation of the Shuswap complex. Finally, since the Joss Mountain P-T-t-d path fits with the thermal state of upper plate during convergence, we tentatively interpret that an oceanic lithosphere subducted beneath paleo-North America during Cordilleran convergence.

#### ACKNOWLEDGMENTS

We acknowledge insightful reviews by Stephen T. Johnston, H. Daniel Gibson, Maria Luisa Crawford, and by Editor Arlo B. Weil, who is also acknowledged for his kind assistance. Andrea Risplendente, Douglas Hall, and Steven Cogswell provided technical assistance on the microprobe and scanning electron microscope. We gratefully acknowledge Sharon D. Carr for patiently guiding Kuiper through the isotope dilution–thermal ionization mass spectrometry (ID-TIMS) process and M. Iole Spalla for reading a first draft of the paper. Funding for this project was provided through various Natural Sciences and Engineering Research Council of Canada (NSERC) grants to Williams and a Programma dell’Università per la Ricerca (PUR) 2009-ATE-0503 grant from the Università degli Studi di Milano. Many samples used for this work were collected by Dennis H. Johnston during his Ph.D. project at the University of New Brunswick.

#### REFERENCES CITED

Adams, M.G., Lentz, D.R., Shaw, C.S.J., Williams, P.F., Archibald, D.A., and Cousens, B., 2005, Eocene shoshonitic mafic dykes intruding the Monashee complex, British Columbia: A petrogenetic relationship with the Kamloops Group volcanic sequence?: *Canadian Journal of Earth Sciences*, v. 42, p. 11–24, doi:10.1139/e04-091.

Armstrong, R.L., Parrish, R.R., van der Heyden, P., Scott, K., Runkle, D., and Brown, R.L., 1991, Early Proterozoic basement exposures in the southern Canadian Cordillera: Core gneiss of Frenchman Cap, Unit 1

of the Grand Forks Gneiss and the Vaseaux Formation: *Canadian Journal of Earth Sciences*, v. 28, p. 1169–1201, doi:10.1139/e91-107.

Beranek, L.P., and Mortensen, J.K., 2011, The timing and provenance record of the Late Permian Klondike orogeny in northwestern Canada and arc-continent collision along western North America: *Tectonics*, v. 30, p. TC5017, doi:10.1029/2010TC002849.

Brodie, K.H., and Rutter, E.H., 1985, On the relationship between rock deformation and metamorphism with special reference to the behaviour of basic rocks, in Thompson, A.B., and Rubie, D.C., eds., *Metamorphic Reactions, Volume 4*: Berlin, Springer Verlag, p. 138–179.

Brown, R.L., 1980, Frenchman Cap Dome, Shuswap Complex, British Columbia: A Progress Report: *Geological Survey of Canada Paper 80-1A*, p. 47–51.

Brown, R.L., and Carr, S.D., 1990, Lithospheric thickening and orogenic collapse within the Canadian Cordillera, in *Proceedings of the Pacific Rim '90 Congress, Brisbane, Australia, 1990, Volume 2*: Australasian Institute of Mining and Metallurgy, p. 1–10.

Brown, R.L., and Read, P.B., 1983, Shuswap terrane of British Columbia: A Mesozoic “core complex”: *Geology*, v. 11, p. 164–168, doi:10.1130/0091-7613(1983)11<164:STOBCA>2.0.CO;2.

Brown, R.L., Carr, S.D., Johnson, B.J., Coleman, V.J., Cook, F.A., and Varsek, J.L., 1992, The Monashee décollement of the southern Canadian Cordillera: A crustal-scale shear zone linking the Rocky Mountain foreland belt to lower crust beneath accreted terranes, in McClay, K.R., ed., *Thrust Tectonics*: London, UK, Chapman and Hall, p. 357–364.

Brown, R.L., Beaumont, C., and Willet, S.D., 1993, Comparison of the Selkirk fan structure with mechanical models: Implications for interpretation of the southern Canadian Cordillera: *Geology*, v. 21, p. 1015–1018, doi:10.1130/0091-7613(1993)021<1015:COTSFS>2.3.CO;2.

Brown, S.R., Gibson, H.D., Andrews, G.D.M., Thorkelson, D.J., Marshall, D.D., Vervoort, J.D., and Rayner, N., 2012, New constraints on Eocene extension within the Canadian Cordillera and identification of Phanerozoic protoliths for footwall gneisses of the Okanagan Valley shear zone: *Lithosphere*, v. 4, no. 4, p. 354–377, doi:10.1130/L199.1.

Caddick, M.J., Konopásek, J., and Thompson, A.B., 2010, Preservation of garnet growth zoning and the duration of prograde metamorphism: *Journal of Petrology*, v. 51, p. 2327–2347, doi:10.1093/petrology/egq059.

Carr, S.D., 1991, Three crustal zones in the Thor-Odin-Pinnacles area, southern Omineca belt, British Columbia: *Canadian Journal of Earth Sciences*, v. 28, p. 2003–2023, doi:10.1139/e91-182.

Carr, S.D., 1992, Tectonic setting and U-Pb geochronology of the Early Tertiary Ladybird leucogranite suite, Thor-Odin–Pinnacles area, southern Omineca belt, British Columbia: *Tectonics*, v. 11, p. 258–278, doi:10.1029/91TC01644.

Carr, S.D., 1995, The southern Omineca belt, British Columbia: New perspectives from the Lithoprobe Geoscience Program: *Canadian Journal of Earth Sciences*, v. 32, p. 1720–1739, doi: 10.1139 /e95-135.

- Carr, S.D., Parrish, R.P., and Brown, R.L., 1987, Eocene structural development of the Valhalla complex, southeastern British Columbia: *Tectonics*, v. 6, p. 175–196, doi:10.1029/TC006i002p00175.
- Cathelineau, M., 1988, Cation site occupancy in chlorites and illites as a function of temperature: *Clay Minerals*, v. 23, p. 471–485, doi:10.1180/claymin.1988.023.4.13.
- Coleman, V.J., 1990, The Monashee Décollement at Cariboo Alp and Regional Kinematic Indicators, Southeastern British Columbia [M.S. thesis]: Ottawa, Ontario, Canada, Carleton University, 112 p.
- Colpron, M., Nelson, J., and Murphy, D.C., 2007, Northern Cordilleran terranes and their interactions through time: *GSA Today*, v. 17, no. 4–5, p. 4–10, doi:10.1130/GSAT01704-5A.1.
- Crowley, J.L., 1997, U-Pb geochronologic constraints on the cover sequence of the Monashee complex, Canadian Cordillera: Paleoproterozoic deposition on basement: *Canadian Journal of Earth Sciences*, v. 34, p. 1008–1022, doi:10.1139/e17-083.
- Crowley, J.L., 1999, U-Pb geochronologic constraints on Paleoproterozoic tectonism in the Monashee complex, Canadian Cordillera: Elucidating an overprinted geologic history: *Geological Society of America Bulletin*, v. 111, p. 560–577, doi:10.1130/0016-7606 (1999)111 <0560 :UPGCOP>2.3.CO;2.
- Crowley, J.L., and Parrish, R.R., 1999, U-Pb isotopic constraints on diachronous metamorphism in the northern Monashee complex, southern Canadian Cordillera: *Journal of Metamorphic Geology*, v. 17, p. 483–502, doi:10.1046/j.1525-1314.1999.00210.x.
- Crowley, J.L., Brown, R.L., and Parrish, R.R., 2001, Diachronous deformation and a strain gradient beneath the Selkirk allochthon, northern Monashee complex, southeastern Canadian Cordillera: *Journal of Structural Geology*, v. 23, p. 1103–1121, doi:10.1016/S0191-8141(00)00179-6.
- Cubley, J.F., and Pattison, D.R.M., 2012, Metamorphism and deformation of the Grand Forks complex: Implications for the exhumation history of the Shuswap core complex, southern British Columbia: *Canadian Journal of Earth Sciences*, v. 49, p. 1329–1363, doi:10.1139 /e2012-066.
- Digel, S.G., Ghent, E.D., Carr, S.D., and Simony, P.S., 1998, Early Cretaceous kyanite-sillimanite metamorphism and Paleocene sillimanite overprint near Mount Cheadle, southeastern British Columbia: Geometry, geochronology, and metamorphic implications: *Canadian Journal of Earth Sciences*, v. 35, p. 1070–1087, doi:10.1139/e98-052.
- Doughty, P.T., Price, R.A., and Parrish, R.R., 1998, Geology and U-Pb geochronology of Archean basement and Proterozoic cover in the Priest River complex, northwestern United States, and their implications for Cordilleran structure and Precambrian continent reconstructions: *Canadian Journal of Earth Sciences*, v. 35, p. 39–54, doi:10.1139/cjes-35-1-39.
- Droop, G.T.R., 1987, A general equation for estimating Fe<sup>3+</sup> concentrations in ferromagnesian silicates and oxides from microprobe analyses, using stoichiometric criteria: *Mineralogical Magazine*, v. 51, p. 431–435, doi:10.1180/minmag.1987.051.361.10.
- Ernst, W.G., and Liou, J.G., 2008, High- and ultrahigh-pressure metamorphism: Past results and future prospects: *The American Mineralogist*, v. 93, p. 1771–1786, doi:10.2138 /am .2008.2940.

- Fyles, J.T., 1970, Structure of the Shuswap metamorphic complex in the Jordan River area, northwest of Revelstoke, British Columbia, in Wheeler, J.O., ed., Structure of the Southern Canadian Cordillera, Volume 6: Geological Association of Canada, p. 87–98.
- Gabrielse, H., Monger, J.W.H., Wheeler, J.O., and Yorath, C.J., 1991, Chapter 2, Part A. Morphogeological belts, tectonic assemblages, and terranes, in Gabrielse, H., and Yorath, C.J., eds., Geology of the Cordilleran Orogen in Canada: Geological Survey of Canada, Geology of Canada, no. 4, p. 15–28.
- Ganguly, J., and Saxena, S.K., 1984, Mixing properties of aluminosilicate garnets: Constraints from natural and experimental data, and applications to geothermo-barometry: *The American Mineralogist*, v. 69, p. 88–97.
- Gehrels, G., Rusmore, M., Woodsworth, G., Crawford, M., Andronicos, C., Hollister, L., Patchett, J., Ducea, M., Butler, R., Klepeis, K., Davidson, C., Friedman, R., Haggart, J., Mahoney, B., Crawford, W., Pearson, D., and Girardi, J., 2009, U-Th-Pb geochronology of the Coast Mountains batholith in north-coastal British Columbia: Constraints on age and tectonic evolution: *Geological Society of America Bulletin*, v. 121, no. 9–10, p. 1341–1361, doi: 10.1130 /B26404.1.
- Gervais, F., 2009, An objective and testable subdivision scheme for the southeastern Canadian Cordillera, in Proceedings of the Cordilleran Tectonics Workshop: Calgary, Alberta, Canada, p. 19–21.
- Gervais, F., and Brown, R.L., 2011, Testing modes of exhumation in collisional orogens: Synconvergent channel flow in the southeastern Canadian Cordillera: *Lithosphere*, v. 3, no. 1, p. 55–75, doi:10.1130/L98.1.
- Gervais, F., Brown, R.L., and Crowley, J.L., 2010, Tectonic implications for a Cordilleran orogenic base in the Frenchman Cap dome, southeastern Canadian Cordillera: *Journal of Structural Geology*, v. 32, p. 941–959, doi:10.1016/j.jsg.2010.05.006.
- Gerya, T.V., Yuen, D.A., and Maresch, W.V., 2004, Thermo-mechanical modelling of slab detachment: *Earth and Planetary Science Letters*, v. 226, p. 101–116, doi:10.1016/j .epsl .2004.07.022.
- Ghent, E.D., Nicholls, J., Stout, M.Z., and Rottenfusser, B., 1977, Clinopyroxene amphibolite boudins from Three Valley Gap, British Columbia: *Canadian Mineralogist*, v. 15, p. 269–282.
- Gibson, H.D., 2003, Structural and Thermal Evolution of the Northern Selkirk Mountains, Southeastern Canadian Cordillera: Tectonic Development of a Regional-Scale Composite Structural Fan [Ph.D. thesis]: Ottawa, Ontario, Canada, Carleton University, 298 p.
- Gibson, H.D., Brown, R.L., and Parrish, R.R., 1999, Deformation-induced inverted metamorphic field gradients: An example from the southeastern Canadian Cordillera: *Journal of Structural Geology*, v. 21, p. 751–767, doi:10.1016/S0191-8141(99)00051-6.
- Gibson, H.D., Brown, R.L., and Carr, S.D., 2005, U-Th-Pb geochronologic constraints on the structural evolution of the Selkirk fan, northern Selkirk Mountains, southern Canadian Cordillera: *Journal of Structural Geology*, v. 27, p. 1899–1924, doi:10.1016/j .jsg .2005.05.014.
- Gibson, H.D., Brown, R.L., and Carr, S.D., 2008, Tectonic evolution of the Selkirk fan, southeastern Canadian Cordillera: A composite Middle Jurassic–Cretaceous orogenic structure: *Tectonics*, v. 27, p. TC6007, doi:10.1029/2007TC002160.

- Gilley, L.D., 1999, The Nature and Timing of Partial Melting in the Shuswap Metamorphic Core Complex: A SHRIMP U-Pb Geochronologic Investigation [B.S. thesis]: Stanford, California, Stanford University, 57 p.
- Goergen, E.T., and Whitney, D.L., 2012, Long length scales of element transport during reaction texture development in orthoamphibole-cordierite gneiss: Thor-Odin dome, British Columbia, Canada: *Contributions to Mineralogy and Petrology*, v. 163, p. 337–352, doi: 10.1007/s00410-011-0671-y.
- Gosso, G., Messiga, B., Rebay, G., and Spalla, M.I., 2010, Interplay between deformation and metamorphism during eclogitization of amphibolites in the Sesia-Lanzo zone of the western Alps: *International Geology Review*, v. 52, no. 10-12, p. 1193–1219, doi: 10.1080/00206810903529646.
- Green, N.L., and Usdansky, S.I., 1986, Toward a practical plagioclase-muscovite thermometer: *The American Mineralogist*, v. 71, no. 9–10, p. 1109–1117.
- Guidotti, C.V., Cheney, J.T., and Conatore, P.D., 1975, Interrelationships between Mg/Fe and octahedral Al content in biotite: *The American Mineralogist*, v. 60, p. 849–853.
- Gulbin, Y.L., 2012, Garnet–biotite geothermometer and estimation of crystallization temperature of zoned garnets from metapelites: I. Reconstruction of thermal history of porphyroblast growth: *Geology of Ore Deposits*, v. 54, no. 8, p. 602–615, doi:10.1134/S1075701512080089.
- Henry, D., Guidotti, C., and Thomson, J., 2005, The Ti-saturation surface for low-to-medium pressure metapelitic biotites: Implications for geothermometry and Ti-substitution mechanisms: *The American Mineralogist*, v. 90, p. 316–328, doi:10.2138/am.2005.1498.
- Hey, M.H., 1954, A new review of chlorites: *Mineralogical Magazine*, v. 30, p. 277–292.
- Hildebrand, R.S., 2009, Did Westward Subduction Cause Cretaceous-Tertiary Orogeny in the North American Cordillera?: *Geological Society of America Special Paper 457*, 71 p.
- Hinchey, A.M., Carr, S.D., McNeill, P.D., and Rayner, N., 2006, Paleocene–Eocene high-grade metamorphism, anatexis and deformation in the Thor-Odin dome, Monashee complex, southeastern British Columbia: *Canadian Journal of Earth Sciences*, v. 43, p. 1341–1365, doi:10.1139/e06-028.
- Hobbs, B.E., Means, W.D., and Williams, P.F., 1976, *An Outline of Structural Geology*: New York, Wiley, 571 p.
- Hobbs, B.E., Ord, A., Spalla, M.I., Gosso, G., and Zucali, M., 2010, The interaction of deformation and metamorphic reactions, in Spalla, M.I., Marotta, A.M., and Gosso, G., eds., *Advances in Interpretation of geological processes: Refinement of Multi-Scale Data and Integration in Numerical Modelling*: Geological Society of London Special Publication 332, p. 189–222.
- Hoisch, T.D., 1989, A muscovite-biotite geothermometer: *The American Mineralogist*, v. 74, no. 5–6, p. 565–572.
- Hoisch, T.D., 1990, Empirical calibration of six geobarometers for the mineral assemblage quartz+muscovite+biotite+plagioclase+garnet: *Contributions to Mineralogy and Petrology*, v. 104, no. 2, p. 225–234, doi:10.1007/BF00306445.

- Holland, T.J.B., and Powell, R., 1998, An internally consistent thermodynamic data set for phases of petrological interest: *Journal of Metamorphic Geology*, v. 16, no. 3, p. 309–343, doi:10.1111/j.1525-1314.1998.00140.x.
- Johnson, B.J., 1994, Structure and Tectonic Setting of the Okanagan Valley Fault System in the Shuswap Lake Area, Southern British Columbia [Ph.D. thesis]: Ottawa, Ontario, Canada, Carleton University, 266 p.
- Johnson, B.J., 2006, Extensional shear zones, granitic melts, and linkage of overstepping normal faults bounding the Shuswap metamorphic core complex, British Columbia: *Geological Society of America Bulletin*, v. 118, no. 3–4, p. 366–382, doi:10.1130/B25800.1.
- Johnson, B.J., and Brown, R.L., 1996, Crustal structure and Early Tertiary extensional tectonics of the Omineca belt at 51°N latitude, southern Canadian Cordillera: *Canadian Journal of Earth Sciences*, v. 33, p. 1596–1611, doi:10.1139/e96-121.
- Johnston, D.H., 1998, Structural and Thermal Evolution of Northwest Thor-Odin Dome, Monashee Complex, Southeastern British Columbia [Ph.D. thesis]: Fredericton, New Brunswick, Canada, University of New Brunswick, 317 p.
- Johnston, D.H., Williams, P.F., Brown, R.L., Crowley, J.L., and Carr, S.D., 2000, Northeastward extrusion and extensional exhumation of crystalline rocks of the Monashee complex, southeastern Canadian Cordillera: *Journal of Structural Geology*, v. 22, p. 603–625, doi:10.1016/S0191-8141(99)00185-6.
- Johnston, S.T., 2008, The Cordilleran ribbon continent of North America: *Annual Review of Earth and Planetary Sciences*, v. 36, p. 495–530, doi:10.1146/annurev.earth.36.031207.124331.
- Journey, J.M., 1986, Stratigraphy, Internal Strain and Thermo-Tectonic Evolution of Northern Frenchman Cap Dome: An Exhumed Duplex Structure, Omineca Hinterland, S.E. Canadian Cordillera [Ph.D. thesis]: Kingston, Ontario, Canada, Queens University, 404 p.
- Journey, J.M., and Brown, R.L., 1986, Major Tectonic Boundaries of the Omineca Belt in Southern British Columbia: A Progress Report: *Geological Survey of Canada Paper 86-1A*, p. 81–88.
- Jowett, E.C., 1991, Fitting iron and magnesium into the hydrothermal chlorite geothermometer, in *Proceedings of the Geological Association of Canada–Mineralogical Association of Canada–Society of Economic Geology Joint Annual Meeting, Program with Abstracts*: Toronto, Canada, Abstract A 16.
- Kaneko, Y., and Miyano, T., 2004, Recalibration of mutually consistent garnet-biotite and garnet-cordierite geothermometers: *Lithos*, v. 73, p. 255–269, doi:10.1016/j.lithos.2003.12.009.
- Kent, D.V., and Irving, E., 2010, Influence of inclination error in sedimentary rocks on the Triassic and Jurassic apparent pole wander path for North America and implications for Cordilleran tectonics: *Tectonics*, v. 115, p. B10103, doi:10.1029/2009JB007205.
- Kleemann, U., and Reinhardt, J., 1994, Garnet-biotite thermometry revisited: The effect of AlVI and Ti in biotite: *European Journal of Mineralogy*, v. 6, p. 925–941.
- Krogh, E.J., 1982, Metamorphic evolution on Norwegian country-rock eclogites, as deduced from mineral inclusions and compositional zoning in garnets: *Lithos*, v. 15, p. 305–321, doi:10.1016/0024-4937(82)90021-4.

Krogh, T.E., 1973, A low contamination method for hydrothermal decomposition of zircon and extraction of U and Pb for isotopic age determinations: *Geochimica et Cosmochimica Acta*, v. 37, p. 485–494, doi:10.1016/0016-7037(73)90213-5.

Kruse, S., and Williams, P.F., 2005, Brittle faulting in the Thor-Odin culmination, Monashee complex, southern Canadian Cordillera: Constraints on geometry and kinematics: *Canadian Journal of Earth Sciences*, v. 42, p. 2141–2160, doi:10.1139/e05-084.

Kruse, S., and Williams, P.F., 2007, The Monashee reflector: Re-examining a Lithoprobe crustalscale reflector in the southern Canadian Cordillera: *Geosphere*, v. 3, no. 1, p. 26–41, doi: 10.1130/GES00049.1.

Kruse, S., McNeill, P.D., and Williams, P.F., 2004, Geological Map of the Thor–Odin Dome, Southern Monashee Complex, BC: [http://www2.unb.ca/earthsciences/faculty/monashee/ThorOdinMapjuly27\\_05.pdf](http://www2.unb.ca/earthsciences/faculty/monashee/ThorOdinMapjuly27_05.pdf) (last accessed 24 July 2014).

Kuiper, Y.D., 2003, Isotopic Constraints on Timing of Deformation and Metamorphism in Thor–Odin, Monashee Complex, Southeastern BC [Ph.D. thesis]: Fredericton, New Brunswick, Canada, University of New Brunswick, 294 p.

Kuiper, Y.D., Williams, P.F., and Kruse, S., 2006, Possibility of channel flow in the southern Canadian Cordillera: A new approach to explain existing data, in Law, R.D., Searle, M.P., and Godin, L., eds., *Channel Flow, Ductile Extrusion and Exhumation in Continental Collision Zones: Geological Society of London Special Publication 268*, p. 589–611.

Kuiper, Y.D., Shields, C.D., Tubrett, M.N., Bennett, V., and Buchwaldt, R., 2014, Age and provenance of a Paleoproterozoic to Devonian Canadian Cordilleran passive margin sequence, Thor-Odin dome, southeastern British Columbia: *Geological Society of America Bulletin*, doi:10.1130/B31031.1.

Laberge, J.D., and Pattison, D.R.M., 2007, Geology of the western margin of the Grand Fork complex: High grade Cretaceous metamorphism followed by Early Tertiary extension of the Granby fault: *Canadian Journal of Earth Sciences*, v. 44, p. 199–228, doi:10.1139/e06-101.

Lane, L.S., 1984, Deformation History of the Monashee Décollement and Columbia River Fault Zone, British Columbia [Ph.D. thesis]: Ottawa, Ontario, Canada, Carleton University, 480 p.

Lane, L.S., Ghent, E.D., Stout, M.Z., and Brown, R.L., 1989, P-T history and kinematics of the Monashee décollement near Revelstoke, British Columbia: *Canadian Journal of Earth Sciences*, v. 26, p. 231–243, doi:10.1139/e89-019.

Lardeaux, J.M., and Spalla, M.I., 1990, Tectonic significance of P-T-t paths in metamorphic rocks: Examples from ancient and modern orogenic belts: *Memorie della Società Geologica Italiana*, v. 45, p. 51–69.

Lardeaux, J.M., and Spalla, M.I., 1991, From granulites to eclogites in the Sesia zone (Italian western Alps): A record of the opening and closure of the Piedmont ocean: *Journal of Metamorphic Geology*, v. 9, p. 35–59, doi:10.1111/j.1525-1314.1991.tb00503.x.

Le Breton, N., and Thompson, A.B., 1988, Fluid-absent (dehydration) melting of biotite in metapelites in the early stages of crustal anatexis: *Contributions to Mineralogy and Petrology*, v. 99, p. 226–237, doi:10.1007/BF00371463.

- Locock, A.J., 2008, An Excel spreadsheet to recast analyses of garnet into end-member components, and a synopsis of the crystal chemistry of natural silicate garnets: *Computers & Geosciences*, v. 34, p. 1769–1780, doi:10.1016/j.cageo.2007.12.013.
- Lorencak, M., Seward, D., Vanderhaeghe, O., Teyssier, C., and Burg, J.P., 2001, Low-temperature cooling history of the Shuswap metamorphic core complex, British Columbia: Constraints from apatite and zircon fission-track ages: *Canadian Journal of Earth Sciences*, v. 38, p. 1615–1625, doi:10.1139/e01-037.
- Ludwig, K.R., 2001, Users' Manual for Isoplot/Ex v.2.49. A Geochronological Toolkit for Microsoft Excel: Berkeley Geochronology Center Special Publication 1a, 53 p.
- Marotta, A.M., and Spalla, M.I., 2007, Permian–Triassic high thermal regime in the Alps: Result of late Variscan collapse or continental rifting? Validation by numerical modeling: *Tectonics*, v. 26, p. TC4016, doi:10.1029/2006TC002047.
- Marotta, A.M., Fernandez, M., and Sabadini, R., 1998, Mantle unrooting in collisional settings: *Tectonophysics*, v. 296, p. 31–46, doi:10.1016/S0040-1951(98)00134-6. McNicoll, V.J., and Brown, R.L., 1995, The Monashee décollement at Cariboo Alp, southern flank of the Monashee complex, southern British Columbia, Canada: *Journal of Structural Geology*, v. 17, no. 1, p. 17–30, doi:10.1016/0191-8141(94)E0028-W.
- Menegon, L., Pennacchioni, G., and Stünitz, H., 2006, Nucleation and growth of myrmekite during ductile shear deformation in metagranites: *Journal of Metamorphic Geology*, v. 24, p. 553–568, doi:10.1111/j.1525-1314.2006.00654.x.
- Monger, J.W.H., Price, R.A., and Tempelman-Kluit, D.J., 1982, Tectonic accretion and the origin of the two major metamorphic and plutonic belts in the Canadian Cordillera: *Geology*, v. 10, p. 70–75, doi:10.1130/0091-7613(1982)10<70:TAATOO>2.0.CO;2.
- Monger, J.W.H., van der Heyden, P., Journeay, J.M., Evenchick, C.A., and Mahoney, J.B., 1994, Jurassic–Cretaceous basins along the Canadian Coast belt: Their bearing on pre–mid-Cretaceous sinistral displacements: *Geology*, v. 22, p. 175–178, doi:10.1130 /0091-7613 (1994) 022<0175:JCBATC>2.3.CO;2.
- Mørk, M.B., 1985, A gabbro eclogite transition of Flemsoy, Suamøre, western Norway: *Chemical Geology*, v. 50, p. 283–310, doi:10.1016/0009-2541(85)90125-1.
- Murphy, D.C., van der Heyden, P., Parrish, R.R., Klepacki, D.W., McMillan, W., Struik, L.C., and Gabites, J., 1995, New geochronological constraints on Jurassic deformation of the western edge of North America, southeastern Canadian Cordillera, in Miller, D.M., and Busby, C., eds., *Jurassic Magmatism and Tectonics of the North American Cordillera: Geological Society of America Special Paper 299*, p. 159–171, doi:10.1130/SPE299-p159.
- Myers, J.S., 1970, Gneiss types and their significance in the repeatedly deformed and metamorphosed Lewisian complex of Western Harris, Outer Hebrides: *Scottish Journal of Geology*, v. 6, p. 186–199, doi:10.1144/sjg06020186.
- Nelson, J.L., Colpron, M., and Israel, S., 2013, The Cordillera of British Columbia, Yukon, and Alaska: Tectonics and metallogeny, in Colpron, M., Bissing, T., Rusk, B.G., and Thompson, J.F.H., eds., *Tectonics, Metallogeny, and Discovery: The North America Cordillera and Similar Accretionary Settings: Society of Economic Geologists Special Publication 17*, p. 53–109.

- Norlander, B.H., Whitney, D.L., Teyssier, C., and Vanderhaeghe, O., 2002, Partial melting and decompression of the Thor-Odin dome, Shuswap metamorphic complex, Canadian Cordillera: *Lithos*, v. 61, p. 103–125, doi:10.1016/S0024-4937(02)00075-0.
- Nyman, M.W., Pattison, D.R.M., and Ghent, E.D., 1995, Melt extraction during formation of K-feldspar + sillimanite migmatites, west of Revelstoke, British Columbia: *Journal of Petrology*, v. 36, no. 2, p. 351–372, doi:10.1093/petrology/36.2.351.
- Okulitch, A.V., 1985, Paleozoic plutonism in southeastern British Columbia: *Canadian Journal of Earth Sciences*, v. 22, p. 1409–1424, doi:10.1139/e85-148.
- Okulitch, A.V., Wanless, R.K., and Loveridge, W.D., 1975, Devonian plutonism in south-central British Columbia: *Canadian Journal of Earth Sciences*, v. 12, p. 1760–1769, doi:10.1139/e75-156.
- Paradis, S., Bailey, S.L., Creaser, R.A., Piercey, S.J., and Schiarizza, P., 2006, Paleozoic magmatism and syngenetic massive sulphide deposits of the Eagle Bay assemblage, Kootenay terrane, southern British Columbia, in Colpron, M., and Nelson, J.L., eds., *Paleozoic Evolution and Metallogeny of Pericratonic Terranes at the Ancient Pacific Margin of North America*, Canadian and Alaskan Cordillera: Geological Association of Canada Special Paper 45, p. 383–414.
- Parkinson, D.L., 1991, Age and isotopic character of early Proterozoic basement gneisses in the southern Monashee complex, southeastern British Columbia: *Canadian Journal of Earth Sciences*, v. 28, p. 1159–1168, doi:10.1139/e91-106.
- Parkinson, D.L., 1992, Age and Tectonic Evolution of the Southern Monashee Complex, Southeastern British Columbia: A Window into the Deep Crust [Ph.D. thesis]: Santa Barbara, California, University of Santa Barbara, 372 p.
- Parrish, R.R., 1987, An improved micro-capsule for zircon dissolution in U-Pb geochronology: *Chemical Geology*, v. 66, p. 99–102.
- Parrish, R.R., 1992, Miscellaneous U-Pb zircon dates from southeast British Columbia: *Geological Survey of Canada Paper 91-2*, p. 143–153.
- Parrish, R.R., 1995, Thermal evolution of the southeastern Canadian Cordillera: *Canadian Journal of Earth Sciences*, v. 32, p. 1618–1642, doi:10.1139/e95-130.
- Parrish, R.R., and Krogh, T.E., 1987, Synthesis and purification of  $^{205}\text{Pb}$  for U-Pb geochronology: *Chemical Geology*, v. 66, p. 103–110.
- Parrish, R.R., Roddick, J.C., Loveridge, W.D., and Sullivan, R.W., 1987, Uranium-Lead Analytical Techniques at the Geochronology Laboratory: *Geological Survey of Canada Paper 87-2*, p. 3–7.
- Parrish, R.R., Carr, S.D., and Parkinson, D.L., 1988, Eocene extensional tectonics and geochronology of the southern Omineca belt, British Columbia and Washington: *Tectonics*, v. 7, no. 2, p. 181–212, doi:10.1029/TC007i002p00181.
- Passchier, C.W., and Trouw, R.A.J., 2005, *Microtectonics*: Berlin, Springer, 366 p.

- Perchuk, L.L., and Lavrent'eva, I.V., 1983, Experimental investigation of exchange equilibria in the system cordierite-garnet-biotite, in Saxena, S.K., ed., *Kinetics and Equilibrium in Mineral Reactions*: New York, Springer-Verlag, p. 199–239.
- Perchuk, L.L., Aranovich, L.Y., Podlesskii, K.K., Lavrent'eva, I.V., Gerasimov, V.Y., Fed'Kin, V.V., Kitsul, V.I., Karasakov, L.P., and Berdnikov, N.V., 1985, Precambrian granulites of the Aldan Shield, eastern Siberia, USSR: *Journal of Metamorphic Geology*, v. 3, no. 3, p. 265–310, doi:10.1111/j.1525-1314.1985.tb00321.x.
- Powell, R., and Holland, T.J.B., 1994, Optimal geothermometry and geobarometry: *The American Mineralogist*, v. 70, p. 120–133.
- Price, R.A., and Mountjoy, E.W., 1970, Geologic structure of the Canadian Rocky Mountains between Bow and Athabasca Rivers—A progress report, in Wheeler, J.O., ed., *Structure of the Southern Canadian Cordillera*: Geological Association of Canada Special Paper 6, p. 7–25.
- Pryer, L.L., and Robin, P.-Y.F., 1996, Differential stress control on the growth and orientation of flame perthite: A palaeostress direction indicator: *Journal of Structural Geology*, v. 18, no. 9, p. 1151–1166, doi:10.1016/0191-8141(96)00037-5.
- Read, P.B., 1980, Stratigraphy and Structure: Thor-Odin to Frenchman Cap “Domes,” Vernon East-Half Map Area, Southern British Columbia: Geological Survey of Canada, Current research part A; Paper: 80-1A, p. 19–25.
- Read, P.B., and Brown, R.L., 1981, The Columbia River fault zone: Southeastern margin of the Shuswap and Monashee complexes, southern British Columbia: *Canadian Journal of Earth Sciences*, v. 18, p. 1127–1145, doi:10.1139/e81-108.
- Rebay, G., Spalla, M.I., and Zanoni, D., 2012, Interaction of deformation and metamorphism during subduction and exhumation of hydrated oceanic mantle: Insights from the western Alps: *Journal of Metamorphic Geology*, v. 30, p. 687–702, doi:10.1111/j.1525-1314.2012.00990.x.
- Reesor, J.E., and Moore, J.M., Jr., 1971, Petrology and Structure of Thor–Odin Gneiss Dome, Shuswap Metamorphic Complex, British Columbia: Geological Survey of Canada Paper 195, 149 p.
- Roddick, J.C., 1987, Generalized numerical error analysis with applications to geochronology and thermodynamics: *Geochimica et Cosmochimica Acta*, v. 51, p. 2129–2135, doi: 10.1016 /0016-7037(87)90261-4.
- Roddick, J.C., Loveridge, W.D., and Parrish, R.R., 1987, Precise U/Pb dating of zircon at the subnanogram Pb level: *Chemical Geology*, v. 66, p. 111–121.
- Ross, G.M., and Parrish, R.R., 1991, Detrital zircon geochronology of metasedimentary rocks in the southern Omineca belt, Canadian Cordillera: *Canadian Journal of Earth Sciences*, v. 28, p. 1254–1270, doi:10.1139/e91-112.
- Scammell, R.J., and Brown, R.L., 1990, Cover gneisses of the Monashee terrane: A record of synsedimentary rifting in the North American Cordillera: *Canadian Journal of Earth Sciences*, v. 27, p. 712–726, doi:10.1139/e90-070.

- Schaubs, P., Carr, S.D., and Berman, R.G., 2002, Structural and metamorphic constraints on ca. 70 Ma deformation of the northern Valhalla complex, British Columbia: Implications for the tectonic evolution of the southern Omineca belt: *Journal of Structural Geology*, v. 24, p. 1195–1214, doi:10.1016/S0191-8141(01)00101-8.
- Schreurs, J., 1985, Prograde metamorphism of metapelites, garnet-biotite thermometry and prograde changes of biotite chemistry in high grade rocks of West Uusimaa, southwest Finland: *Lithos*, v. 18, p. 69–80, doi:10.1016/0024-4937(85)90011-8.
- Sigloch, K., and Mihalyuk, M.G., 2013, Intra-oceanic subduction shaped the assembly of Cordilleran North America: *Nature*, v. 496, p. 50–56, doi:10.1038/nature12019.
- Simony, P.S., and Carr, S.D., 1997, Large lateral ramps in the Eocene Valkyr shear zone: Extensional ductile faulting controlled by plutonism in southern British Columbia: *Journal of Structural Geology*, v. 19, no. 6, p. 769–784, doi:10.1016/S0191-8141(97)00011-4.
- Simony, P.S., and Carr, S.D., 2011, Cretaceous to Eocene evolution of the southeastern Canadian Cordillera: Continuity of Rocky Mountain thrust systems with zones of “in-sequence” mid-crustal flow: *Journal of Structural Geology*, v. 33, p. 1417–1434, doi:10.1016/j.jsg.2011.06.001.
- Spalla, M.I., and Gosso, G., 1999, Pre-Alpine tectono-metamorphic units in the central southern Alps: Structural and metamorphic memory, in *Proceedings of the 3rd Workshop on Alpine Geological Studies*, Oropa, Biella, Italy, 1999: *Memorie di Scienze Geologiche Padova* 51, p. 221–229.
- Spalla, M.I., and Marotta, A.M., 2007, P-T evolution vs. numerical modelling: A key to unravel the Paleozoic to early Mesozoic tectonic evolution of the Alpine area: *Periodico di Mineralogia*, v. 76, p. 267–308.
- Spalla, M.I., Siletto, G.B., di Paola, S., and Gosso, G., 2000, The role of structural and metamorphic memory in the distinction of tectono-metamorphic units: The basement of the Como Lake in the southern Alps: *Journal of Geodynamics*, v. 30, no. 1–2, p. 191–204, doi: 10.1016 /S0264-3707(99)00033-2.
- Spalla, M.I., Zucali, M., di Paola, S., and Gosso, G., 2005, A critical assessment of the tectonothermal memory of rocks and definition of the tectono-metamorphic units: Evidence from fabric and degree of metamorphic transformations, in *Gapais, D., Brun, J.P., and Cobbold, P.R., eds., Deformation Mechanisms, Rheology and Tectonics: From Minerals to the Lithosphere: Geological Society of London Special Publication* 243, p. 227–247.
- Spalla, M.I., Zanoni, D., Williams, P.F., and Gosso, G., 2011, Deciphering cryptic P-T-d-t histories in the western Thor-Odin dome, Monashee Mountains, Canadian Cordillera: A key to unravelling pre-Cordilleran tectonic signatures: *Journal of Structural Geology*, v. 33, p. 399–421, doi:10.1016/j.jsg.2010.11.014.
- Spark, R.N., 2001, *Crustal Thickening and Tectonic Denudation within the Thor-Odin Culmination, Monashee Complex, Southern Canadian Cordillera* [Ph.D. thesis]: Fredericton, New Brunswick, Canada, University of New Brunswick, 383 p.
- Spear, F.S., 1993, *Metamorphic Phase Equilibria and Pressure-Temperature-Time Paths*: Chelsea, Michigan, BookCrafters, Inc., 799 p.
- Spear, F.S., and Cheney, J.T., 1989, A petrogenetic grid for pelitic schist in the system SiO<sub>2</sub>-Al<sub>2</sub>O<sub>3</sub>-FeO-MgO-K<sub>2</sub>O-H<sub>2</sub>O: *Contributions to Mineralogy and Petrology*, v. 101, p. 149–164, doi:10.1007/BF00375302.

- Spear, F.S., Kohn, M.J., and Cheney, J.T., 1999, P-T paths from anatectic pelites: Contributions to Mineralogy and Petrology, v. 134, p. 17–32, doi:10.1007/s004100050466.
- Stacey, J.S., and Kramers, J.D., 1975, Approximation of terrestrial lead isotope evolution by a two-stage model: Earth and Planetary Science Letters, v. 26, p. 207–221, doi:10.1016/0012-821X(75)90088-6.
- Steiger, R.H., and Jäger, E., 1977, Subcommittee on Geochronology: Convention on the use of decay constants in geo- and cosmochronology: Earth and Planetary Science Letters, v. 36, p. 359–362, doi:10.1016/0012-821X(77)90060-7.
- Vernon, R.H., 2004, A Practical Guide to Rock Microstructure: Cambridge, UK, Cambridge University Press, 594 p.
- Wanless, R.K., and Reesor, J.E., 1975, Precambrian zircon age of orthogneiss in the Shuswap metamorphic complex, British Columbia: Canadian Journal of Earth Sciences, v. 12, p. 326–332, doi:10.1139/e75-028.
- White, R.W., Powell, R., and Holland, T.J.B., 2001, Calculation of partial melting equilibria in the system Na<sub>2</sub>O-CaO-K<sub>2</sub>O-FeO-MgO-Al<sub>2</sub>O<sub>3</sub>-SiO<sub>2</sub>-H<sub>2</sub>O (NCKFMASH): Journal of Metamorphic Geology, v. 19, p. 139–153, doi:10.1046/j.0263-4929.2000.00303.x.
- Whitney, D.L., and Evans, B.W., 2010, Abbreviations for names of rock-forming minerals: The American Mineralogist, v. 95, p. 185–187, doi:10.2138/am.2010.3371.
- Williams, P.F., and Jiang, D., 2005, An investigation of lower crustal deformation: Evidence for channel flow and its implications for tectonics and structural studies: Journal of Structural Geology, v. 27, p. 1486–1504, doi:10.1016/j.jsg.2005.04.002.
- Wu, C.M., and Zhao, G., 2006, Recalibration of the garnet-muscovite (GM) geothermometer and the garnet-muscovite-plagioclase-quartz (GMPQ) geobarometer for metapelitic assemblages: Journal of Petrology, v. 47, no. 12, p. 2357–2368, doi:10.1093/petrology/egl047.
- Wu, C.M., Zhang, J., and Ren, L.D., 2004, Empirical garnet-biotite-plagioclase-quartz (GBPQ) geobarometry in medium- to high-grade metapelites: Journal of Petrology, v. 45, no. 9, p. 1907–1921, doi:10.1093/petrology/egh038.
- Yardley, B.W.D., 1977, An empirical study of diffusion in garnet: The American Mineralogist, v. 62, p. 793–800. York, D., 1968, Least squares fitting of a straight line with correlated errors: Earth and Planetary Science Letters, v. 5, p. 320–324, doi:10.1016/S0012-821X(68)80059-7.
- Zanoni, D., Spalla, M.I., and Gosso, G., 2010, Vestiges of lost tectonic units in conglomerate pebbles? A test in Permian sequences of the Southalpine Orobic Alps: Geological Magazine, v. 147, no. 1, p. 98–122, doi:10.1017/S0016756809990252.
- Zucali, M., 2005, JPT—Mineral Formula Calculation and Geo-Thermobarometry: <http://michelezucali.wix.com/michelezucali#!jpt/c1khr> (last accessed 24 July 2014).
- Zwart, H.J., 1962, On the determination of polymetamorphic mineral associations and its application to the Bosost area (central Pyrenees): Geologische Rundschau, v. 52, p. 38–65, doi: 10.1007/BF01840064.

Figure 1. Geological sketch map of the Shuswap metamorphic complex of the Omineca belt at the latitude of the Thor-Odin culmination (modified after Carr, 1991). Rectangle with the thick outline locates Figure 2. Inset map shows the five belts constituting the Canadian Cordillera according to Gabrielse et al. (1991); RMT—Rocky Mountain trench; FRF—Fraser River fault.

Figure 2. Geological map of the Joss Mountain domain modified after Johnston et al. (2000) and Kruse et al. (2004). Locations of samples used for mineral chemistry, pressure-temperature (P-T) estimates, and U-Pb geochronology are shown. Wm—white mica; Bt—biotite; Cal—calcite; Di—diopside; Fsp—feldspar; Grt—garnet; Pl—plagioclase; Sil—sillimanite; Tr—tremolite; Wo—wollastonite; Qz—quartz.

Figure 3. Summary of pressure-temperature (P-T) estimates available for the Thor-Odin culmination. Legend: 1—sillimanite-bearing migmatites from Three Valley Gap (Nyman et al., 1995); 2—clinopyroxene-garnet-bearing amphibolites from Three Valley Gap (Ghent et al., 1977); samples from Bearpaw Lake and Saturday Peak: 3—gedrite-cordierite rocks, 4—metapelitic rocks, 5a—garnet-amphibole-bearing rocks, Ti-oxide-free, and 5b—garnet-amphibole-bearing rocks with Ti-oxides (Norlander et al., 2002); 6—peak conditions in orthoamphibole-cordierite gneiss boudins from the southern Thor-Odin culmination (Goergen and Whitney, 2012); pressure-temperature-deformation-time (P-T-d-t) path from the transect throughout Blanket Mountain and Greenbush shear zone: 7—metapelites, 8—metabasites (Spalla et al., 2011). ST—transposition foliation.7 Figure 4. (A) Lithostratigraphy transposed into ST; metapelitic schist (gray) interlayered with marbles (whitish). Picture taken some 500 m south of Joss Mountain top, looking WNW-ward. (B) Impure marble layer recording an F2 intrafolial fold within ST. Picture taken on the eastern slope, just below Joss Mountain top. Hammer for scale. (C) Two E-W-trending pegmatite dikes (sample 4) crosscutting orthogneiss, marble, and metapelitic schist. Picture taken from the east side of Joss Mountain, looking to the WNW. The width of the photograph is about 400 meters. (D) Contact of the dated pegmatite (sample 4), crosscutting the foliation in the host metapelitic schist. Viewing direction is down to the ENE. Compass for scale.

Figure 5. Microstructures from white mica (Wm)-bearing schist. Mineral compositional variations are shown in Figures 8, 9, and 10 and Table 1. (A) Centimeter-sized WmI porphyroclast wrapped by ST defined by BtII, WmII, and Qz; crossed polars. The backscattered electron image in the inset shows Sil crystals overgrowing WmI. (B) Pod consisting of Qz and KfsI porphyroclast wrapped by WmII and BtII marking ST; crossed polars. (C) Intrafolial microfold within ST. BtII and WmII are parallel to the microfold axial plane; a post-STa microshear, defined by BtIII and Sil, intersects BtII and WmII films that define ST and deflects around the Qz-bearing microfold hinge; plane polarized light. (D) Two-growth-stage Grt porphyroblast. The inner part of the porphyroblast (GrtI) contains a straight internal foliation that is oblique to the external ST; the outer part of the porphyroblast (GrtII) contains a few inclusions aligned along the internal foliation, which progressively grew into parallelism with the external ST; white dotted line separates the interpreted inclusion-rich GrtI and inclusion-poor GrtII parts of the porphyroblast; crossed polars. WmI porphyroclasts are also wrapped by ST, defined by BtII and WmII. The inset shows the internal foliation defined by PlI, BtI, WmI, and Qz in the core of the Grt porphyroblast; crossed polars. (E) Fine-grained GrtII, BtII, WmII, PlIII, and Qz marking ST foliation; a WmIII lath overgrew BtII at a high angle; plane polarized light. (F) Coronitic Sil and minor BtIII, which grew at the expense of WmII and Grt porphyroblast. (G) BtII partially replaced by KfsIII, ChI, and minor Fe-oxides (white spots); backscattered electron image. (H) Post-STb microshear intersecting ST defined by WmII and BtII; plane polarized light. The inset (backscattered electron image; black bar = 0.1 mm) shows that this microshear is defined by ChI, WmIII, and minor KfsIII, Ab, and Rt. Mineral abbreviations are according to Whitney and Evans (2010) with the exception of Wm (white mica). ST—transposition foliation.

Figure 6. Microstructures from Bt-bearing schist. Variation in mineral composition is shown in Figures 8, 9, and 10 and Table 1. (A) ST foliation defined by BtII and PIII wrapping millimeter-sized Grt porphyroblasts with an internal foliation (highlighted by dashed and dotted white line) defined mainly by BtI and Ilm; in the inner part of the porphyroblast (GrtI), the internal foliation is at high angle to the external ST, whereas in the outer part (GrtII), it is bent into parallelism and continuous with the external ST. Thin dashed white line marks the interpreted boundary between GrtI and II. One-millimeter-thick corona of PIII rims Grt porphyroclasts; plane polarized light. (B) Skeletal centimeter-sized GrtII porphyroblast enclosing a Qz-bearing foliation continuous with and slightly oblique to the external ST, which is defined by BtII, PIII, and Qz; crossed polars. (C) Backscattered electron image showing close-up of a GrtI core enclosing Ilm marking an internal foliation and inclusions of BtI, PII, and Qz. (D) Rim of PIII around a Grt margin that encloses a Qz-bearing foliation at a high angle with the external ST foliation. BtII, PIII, and Qz define rock matrix ST foliation. PIII grains show growth twinning and are mostly unstrained, whereas PIII in the rock matrix does show some internal deformation; crossed polars. (E) Thin rim of PIII replacing the contact between GrtII and BtII; backscattered electron image. (F) ST-parallel compositional layering affected by centimeter-sized F3 fold; BtII is parallel to ST, whereas a few BtII3 grains are parallel to F3 fold axial-planar incipient foliation, which is marked by white dashed line in layers where it is more developed; plane polarized light. Mineral abbreviations are according to Whitney and Evans (2010) with the exception of Wm (white mica). ST—transposition foliation.

Figure 7. Microstructure from orthogneiss and pegmatite. (A) Lattice preferred orientation (LPO) and shape preferred orientation (SPO) of biotite (Bt) defining ST in orthogneiss; fine-grained Wm overprints Kfs; crossed polars. (B) In orthogneiss, SPO of Bt laths and weak SPO Kfs and Pl defines ST; Pl shows polysynthetic twinning; Zrn is found as euhedral to subrounded crystals; crossed polars. (C) Myrmekite between Pl and Kfs in pegmatite; crossed polars. (D) Faint flame perthite in Kfs phenocryst in pegmatite; crossed polars. Mineral abbreviations are according to Whitney and Evans (2010) with the exception of Wm (white mica). ST—transposition foliation.

Figure 8. Compositional variation of white mica and biotite. Mineral proportional formulae are recalculated on the basis of 22 oxygen atoms. Data are separated by rock type (filled circles—white mica [Wm]—bearing schist; open squares—biotite [Bt]—bearing schist), growth generation (black—pre-ST; dark gray—syn-ST; gray—post-STa; light gray—post-STb). Sample locations are shown in Figure 2. (A) Composition of white mica is represented in Al vs. Fe + Mg vs. Si ternary diagram and XM versus XPg binary diagram. (B) Composition of biotite is represented in AlVI vs. Ti binary diagram and AlVI + Ti vs. Fe + Mn vs. Mg ternary diagram; on the binary diagram, the temperature field as a function of Ti and AlVI content in biotite (Schreurs, 1985) is reported. Cation quantities are in atoms per formula unit (a.p.f.u.). ST—transposition foliation.

Figure 9. Variation of garnet composition; mineral proportional formula is recalculated on the basis of 12 oxygen atoms and end-member fraction after Locock (2008). Data are separated by rock type (filled circles—white mica [Wm]—bearing schist; open squares—biotite [Bt]—bearing schist), growth generation (black—pre-ST; dark gray—syn-ST). Sample locations are shown in Figure 2. (A) Prp (pyrope) vs. Alm (almandine) vs. Grs (grossular) and Grs (grossular) vs. Sps (spessartine) vs. Alm (almandine) ternary diagrams. From GrtI to GrtII, there is a slight increase in Alm, which is more marked in Bt-bearing schist; Grt in Bt-bearing schist is relatively enriched in Grs versus the Grt in Wm-bearing schist. (B) Example of compositional variation from core to rim in a Grt porphyroblast from Wm-bearing schist; interpreted boundary between GrtI and GrtII is marked by a black and white dashed line in the chemical profile diagram and photomicrograph respectively; photomicrograph taken in plane polarized light. Cation quantities are in

atoms per formula unit (a.p.f.u.). Mineral abbreviations are according to Whitney and Evans (2010) with the exception of Wm (white mica). ST—transposition foliation.

Figure 10. Compositional variation of feldspar and chlorite. Mineral proportional formulae are recalculated on the basis of 8 and 28 oxygen atoms for feldspar and chlorite, respectively. For feldspar, data are separated by rock type (filled circles—white mica [Wm]—bearing schist; open squares—biotite [Bt]—bearing schist), growth generation (black—pre-ST; dark gray—syn-ST; gray—post-STa; light gray—post-STb). Sample locations are shown in Figure 2. (A) Composition of feldspar in Ab vs. Or vs. An ternary diagram. From PlI to PlIII in Wm-bearing schist, An decreases, whereas in Bt-bearing schist, Pl shows a fairly constant composition; Pl in Bt-bearing schist is richer in An than Pl in Wm-bearing schist. (B) Composition of chlorite in Fe/(Fe + Mg) vs. Si binary diagram. Cation quantities are in atoms per formula unit (a.p.f.u.). Mineral abbreviations are according to Whitney and Evans (2010) with the exception of Wm (white mica). ST—transposition foliation.

Figure 11. (A) Concordia plot for the Joss Mountain orthogneiss (sample 123) with two representative examples of zircon backscattered electron (BSE) images (images are not from the analyzed grains). See text for discussion. Dark part on the right side of zircon image 2 is dirt on the grain mount. (B) Concordia plot and representative BSE images of zircon and monazite (not the grains that are analyzed) from the crosscutting pegmatite at Joss Mountain (sample 4). The photomicrograph of monazite M1 was taken in alcohol in a petri dish under a transmitting light microscope. All scale bars are 50  $\mu$ m.

Figure 12. Pressure-temperature (P-T) conditions for the re-equilibration stages of the white mica (Wm)—bearing schist and biotite (Bt)—bearing schist from Joss Mountain. Reaction curves labeled in italics are from the literature:  $Ms + Ab + Qz = Kfs + Als + L$  (Le Breton and Thompson, 1988);  $Bt + Als = Grt + Crd$  (Spear and Cheney, 1989);  $Ms = Crn + Kfs + H_2O$  (Spear, 1993);  $Kfs + Bt + Mu + H_2O = Grt + L$  (White et al., 2001). Reaction curves labeled with regular characters are calculated with THERMOCALC (Holland and Powell, 1998) on the basis of calculated end-member activity for phases from Wm-bearing schist. Metamorphic facies (Ernst and Liou, 2008): GS—greenschist; EA—epidote-amphibolite facies; AM—amphibolite; HGR—high-pressure granulite; GR—granulite. Light-gray field indicates the P-T conditions for transposition (ST) development considering the retrograde path yielded by assemblages in the core of the garnet as part of the transposition. Dark-gray line is the inferred pressure-temperature-deformation-time (P-T-d-t) path for the Joss Mountain schist; the prograde path is marked by a dashed line and is interpreted as predating the earlier ST P-T conditions recorded in the Bt-bearing schist. Mineral abbreviations are according to Whitney and Evans (2010) with the exception of Wm (white mica).

Figure 13. (A) Comparison between the pressure-temperature-deformation-time (P-T-d-t) path (thin gray line—metapelites; thin black line—metabasites) of the northwestern part of the Thor-Odin culmination (Spalla et al., 2011) and that of the Joss Mountain domain (thick black line). Small and italic characters refer to the P-T-d-t paths in the northwestern Thor-Odin culmination, and large and bold characters refer to the P-T-d-t path of the Joss Mountain domain. (B, C, D) Comparison of the P-T-d-t path of Joss Mountain with the geotherms calculated by Spalla and Marotta (2007) for ongoing subduction (B), for ongoing collision (C), and for orogenic collapse (D). The P-T fields for upper-plate (light gray) and lower-plate (dark gray) geotherms are distinct for subduction and collision stages, and dashed lines indicate geotherms at different distances from the suture zone. Lower and upper-plate geotherms are undifferentiated for postorogenic collapse because they are overlapped. And—andalusite; Ky—kyanite; Sil—sillimanite.

TABLE 1. COMPOSITION OF MINERAL PHASES IN WM- AND BT-BEARING SCHIST Note: Wm—white mica; Bt—biotite. Cations are expressed in atoms per formula unit (a.p.f.u.), whereas molar fractions and feldspar end members are normalized to one. The maximum and minimum values (first line of table boxes) and average with standard deviation (second line of the table box) are reported for each mineral generation. Samples of Wm-bearing schist are: 8, 13, 42, 52, and 55; samples of Bt-bearing schist are 44 and 46; see Figure 2 for sample locations. Mineral proportional formulae on the basis of: 22 oxygen atoms for biotite and white mica, 12 oxygen atoms for garnet, 8 oxygen atoms for feldspar, and 28 oxygen atoms for chlorite. Fe<sup>3+</sup> was recalculated for garnet only. Mineral abbreviations are according to Whitney and Evans (2010) with the exception of Wm (white mica).

TABLE 2. ID-TIMS DATA

TABLE 3. SUMMARY OF THERMOBAROMETRIC ESTIMATES BY INDEPENDENT THERMOBAROMETERS Note: Wm—white mica; Bt—biotite. Ti in Bt—Ti content in biotite (Henry et al., 2005); GB—Fe-Mg exchange reaction between garnet and biotite by (1) Perchuk and Lavrent'eva (1983), (2) Perchuk et al. (1985), (3) Kaneko and Miyano (2004), (4) Ganguly and Saxena (1984), (5) Kleemann and Reinhardt (1994); PW—Na-K exchange reaction between plagioclase and muscovite (Green and Usdansky, 1986); BW—exchange of Mg-Tschermak component between biotite and white mica (Hoisch, 1989); AlIV in Chl—AlIV content in chlorite (Cathelineau, 1988); AlIV and XFe in Chl—AlIV content and XFe ratio in chlorite (Jowett, 1991); AvPT—average pressure-temperature (P-T) calculation method (Powell and Holland, 1994). GBPQ—equilibrium between garnet, biotite, plagioclase, and quartz (1) by Wu et al. (2004), (2) by Hoisch (1990); GWPQ—equilibrium between garnet, white mica, plagioclase, and quartz (Wu and Zhao, 2006); GBWPQ—equilibrium between garnet, biotite, white mica, plagioclase, and quartz (Hoisch, 1990). n = number of estimates.

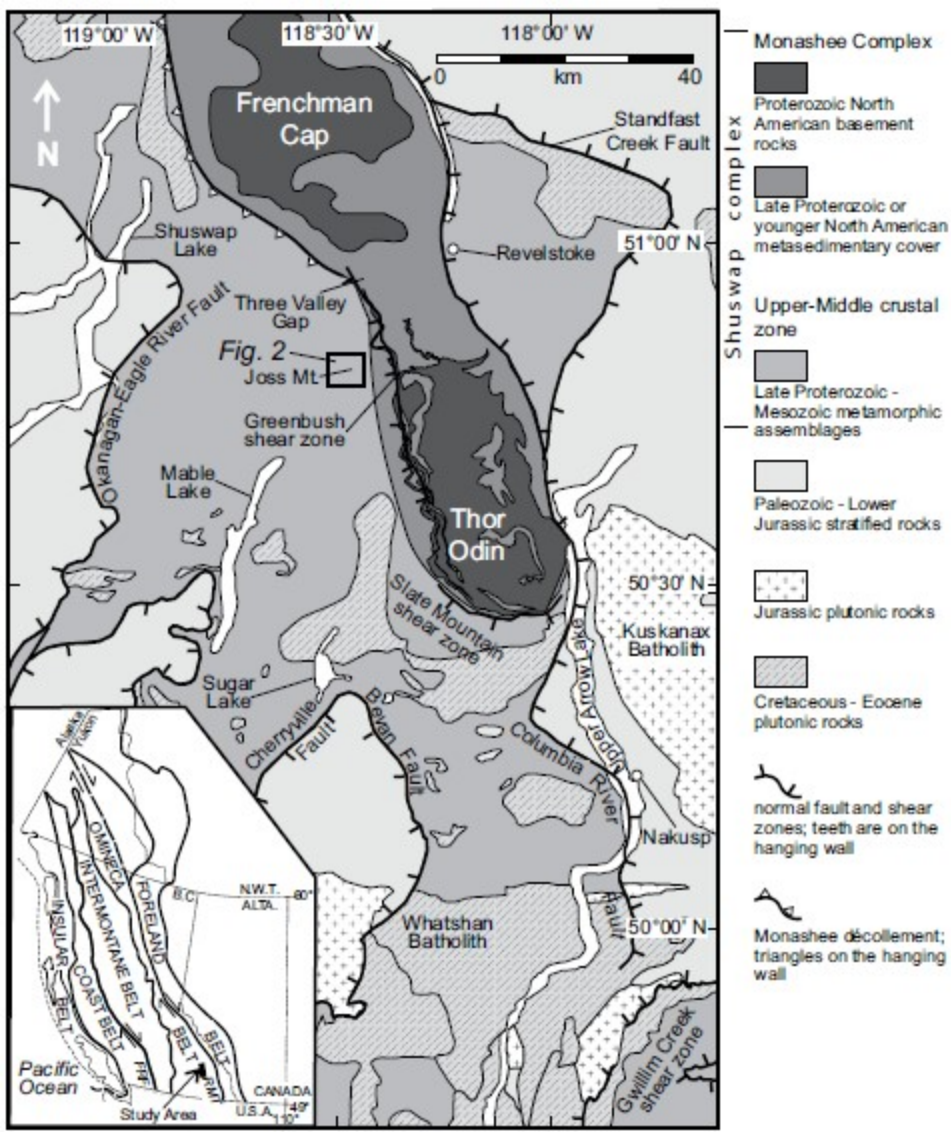
TABLE 4. VARIATION OF CONDITIONS DURING DEVELOPMENT OF TECTONIC STAGES Note: Average pressure (Av P), temperature (Av T), pressure/temperature ratio (Av P/T), depth (Av D), and temperature/depth ratio (Av T/D) for the successive deformation stages in Wm- and Bt-bearing schist. Wm—white mica; Bt—biotite. Pre-ST is the condition for the assemblage yielding the retrograde path. Depth is estimated taking into account an average density for the continental crust of 2.9 g/cm<sup>3</sup> (Spear, 1993).

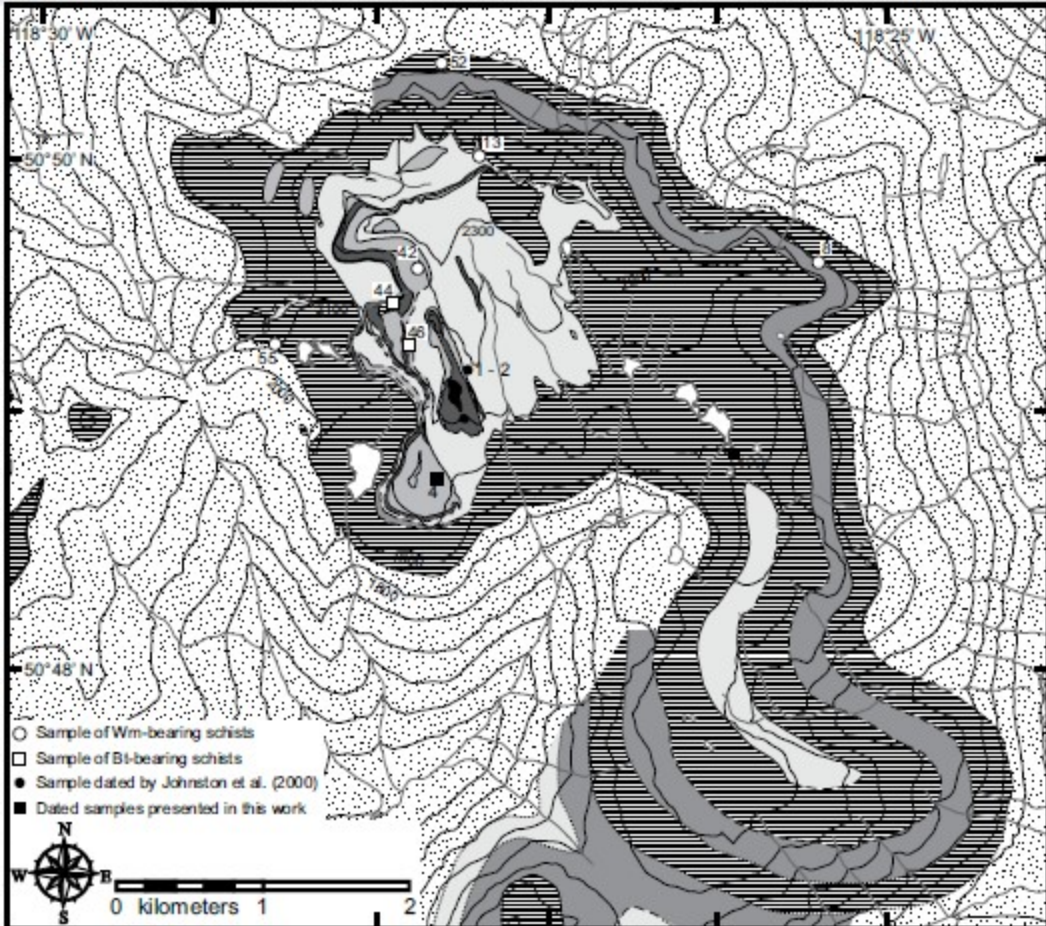
MANUSCRIPT RECEIVED 4 NOVEMBER 2013

REVISED MANUSCRIPT RECEIVED 24 MARCH 2014

MANUSCRIPT ACCEPTED 31 JULY 2014

Printed in the USA





#### Plutonic and metaplutonic rocks

Undifferentiated plutonic and metaplutonic rocks including leucogranite, granitic orthogneiss, and Bt-Sil orthogneiss.

#### Cover Sequence (Proterozoic to Paleozoic?)

Marble.

Pelitic and semipelitic schist and gneiss. Commonly containing Bt, Wm, Grt, Sil.

Calc-silicate gneiss, comprising Cal, Di, Pl, Tr, Wo, and Qz.

Undifferentiated paragneiss comprising calc-silicate gneiss, marble, and pelitic schist.

Quartzite, and/or Wm quartzite.

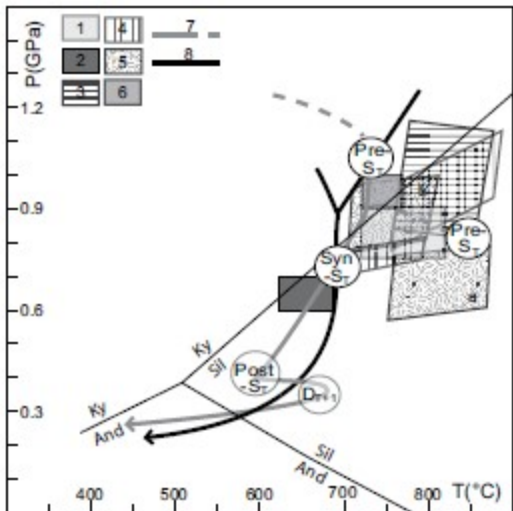
Faserkiesel gneiss, Qz, Fsp, Wm and Sil (pods).

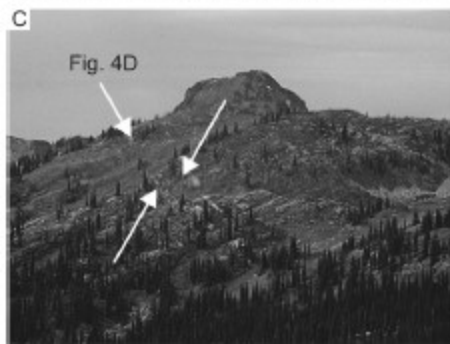
Contacts

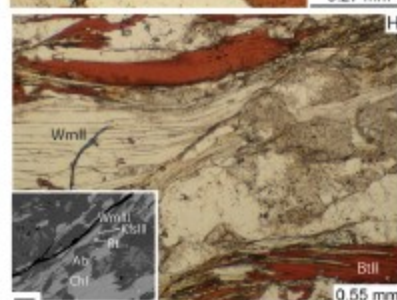
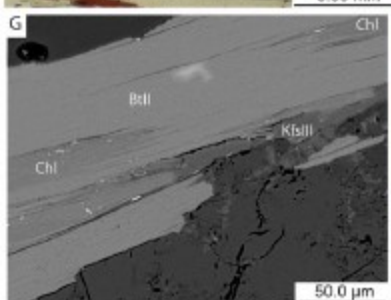
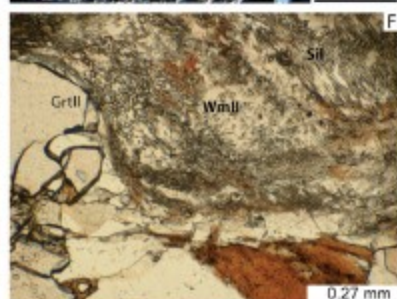
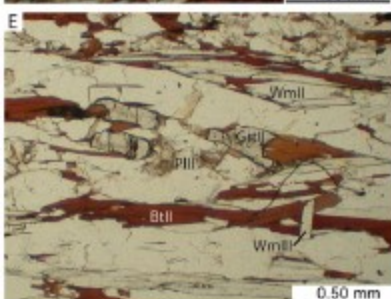
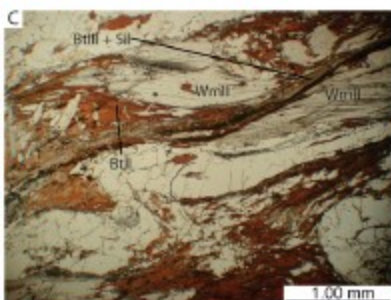
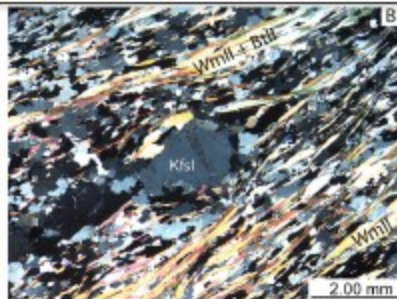
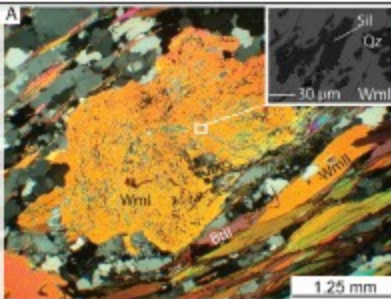
Defined

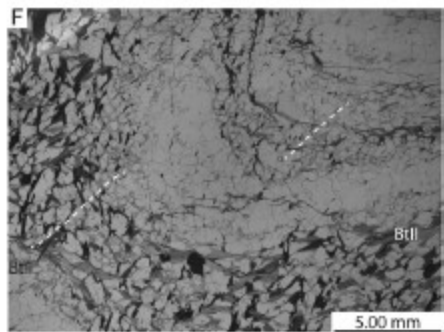
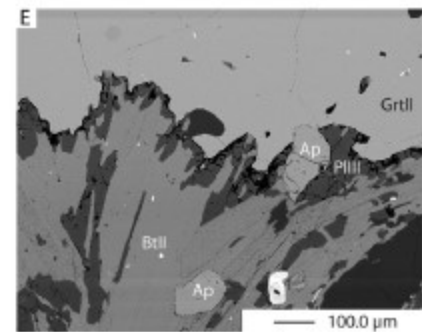
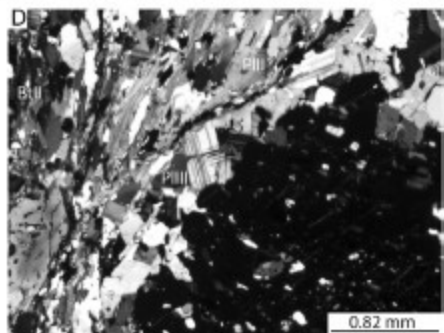
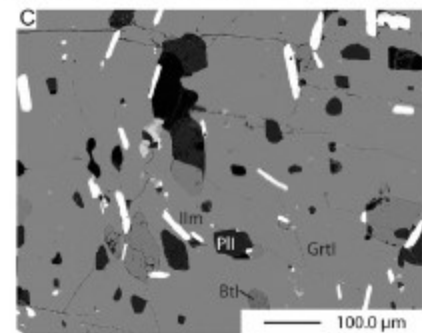
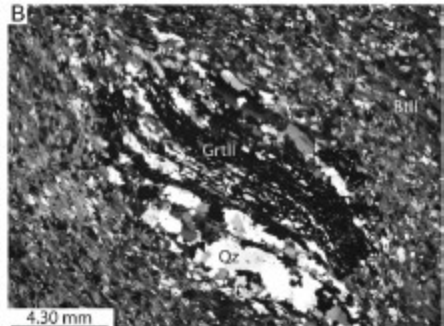
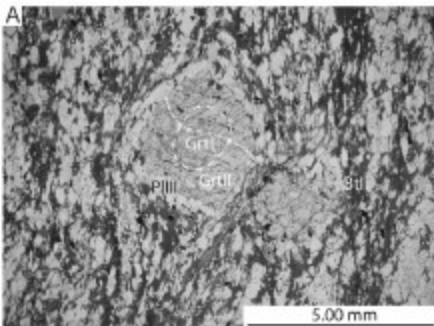
Approximate

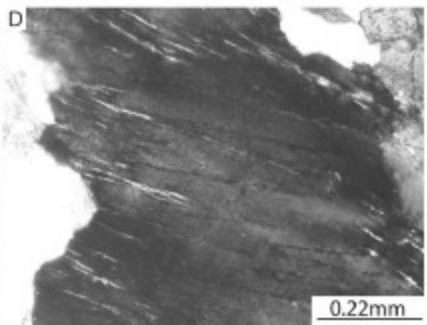
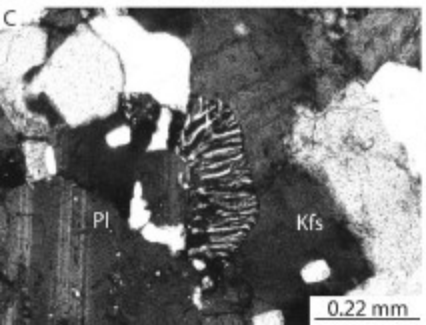
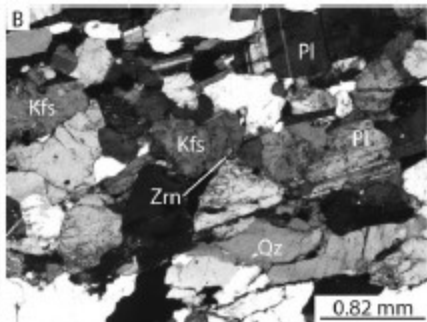
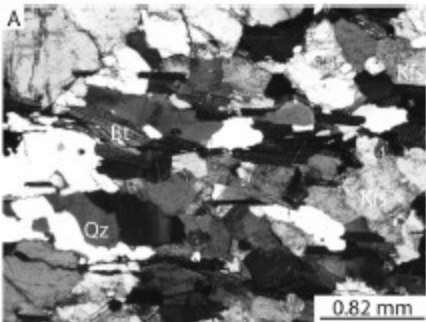
Interpreted

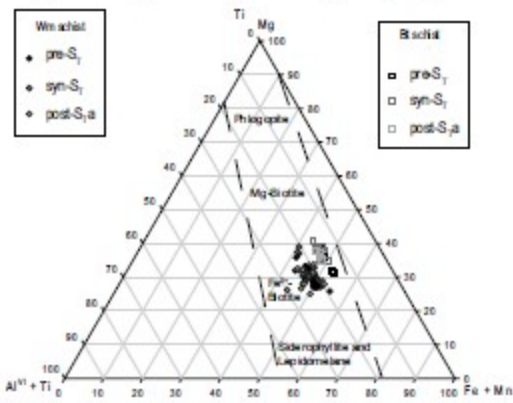
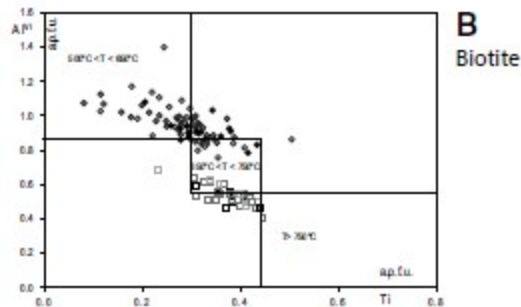
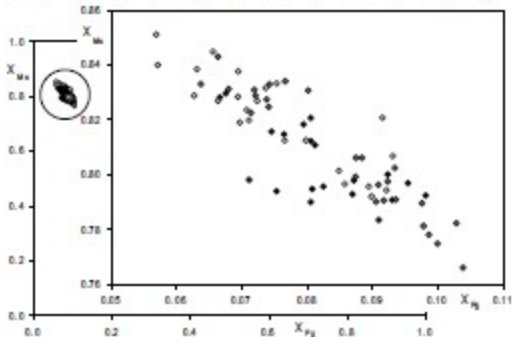
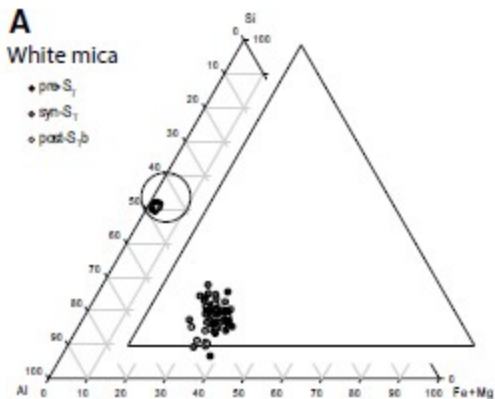


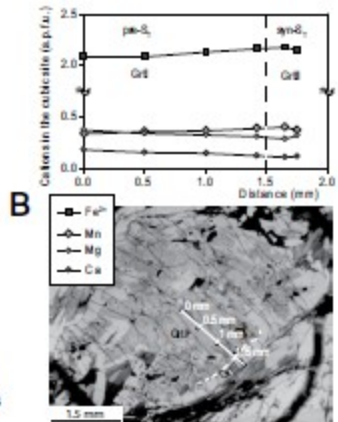
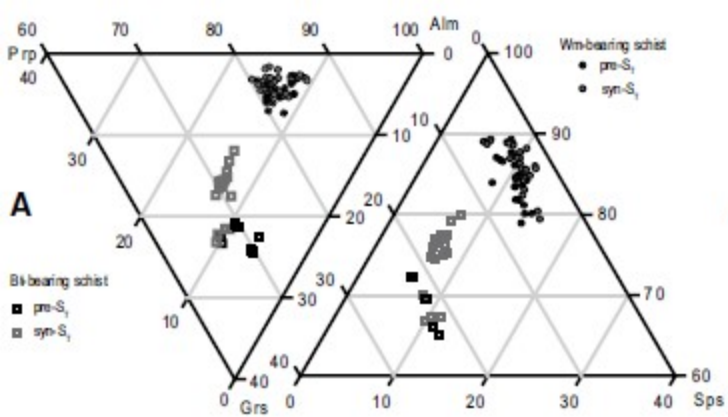












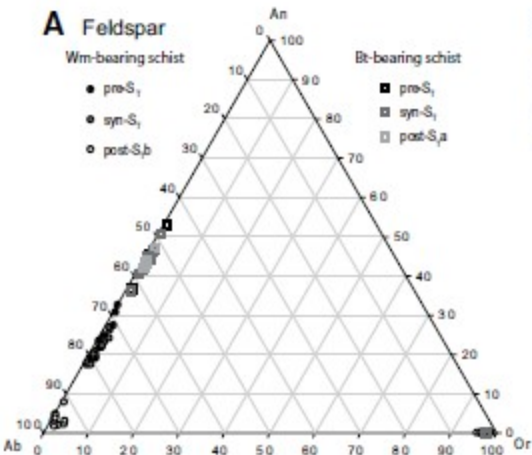
# A Feldspar

Wm-bearing schist

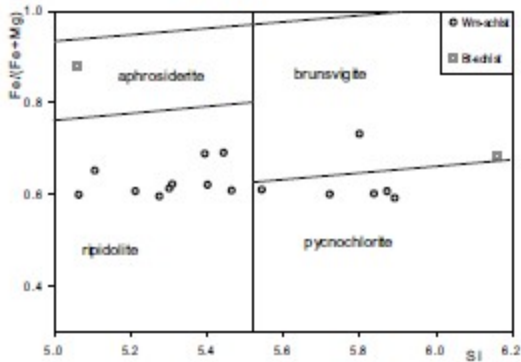
- pre-S<sub>1</sub>
- syn-S<sub>1</sub>
- post-S<sub>1b</sub>

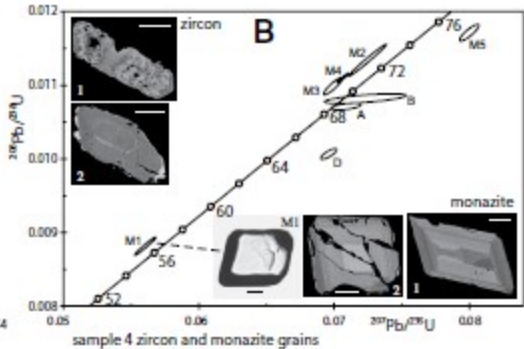
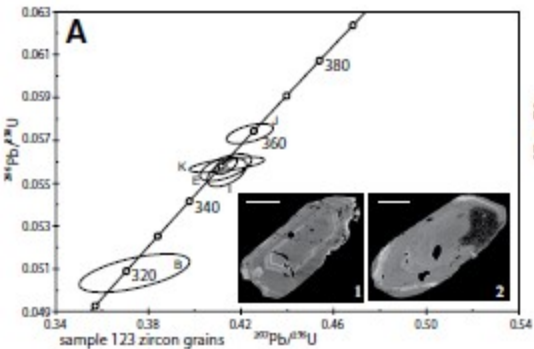
Bt-bearing schist

- pre-S<sub>1</sub>
- ▣ syn-S<sub>1</sub>
- ▤ post-S<sub>1a</sub>



# B Chlorites







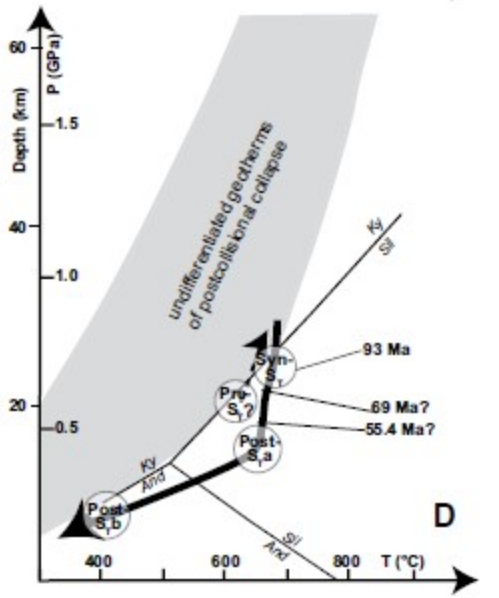
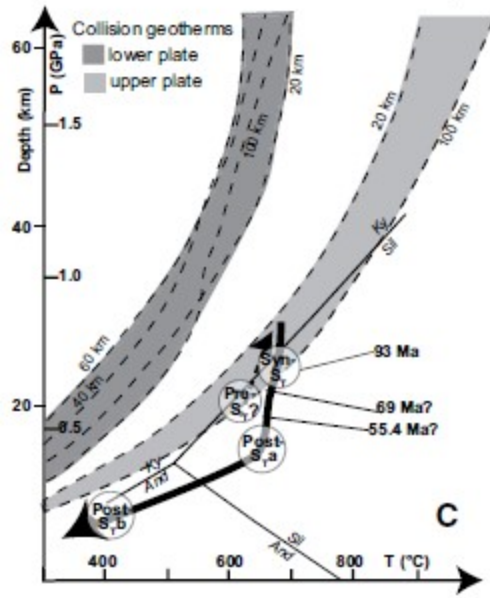
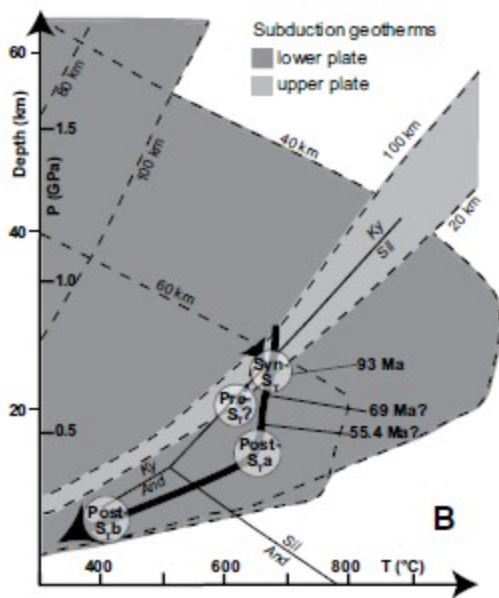
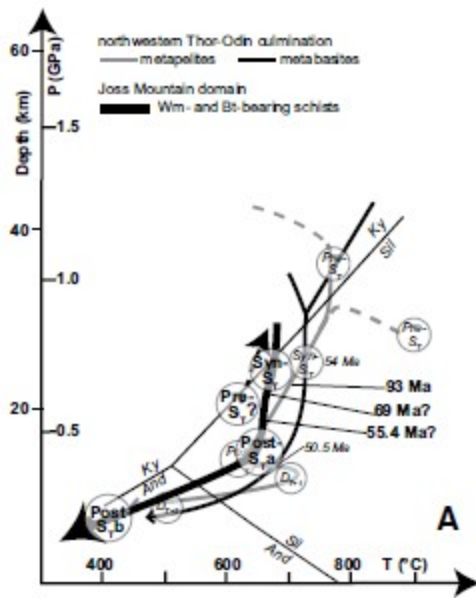


TABLE 1. COMPOSITION OF MINERAL PHASES IN WM- AND BT-BEARING SCHIST

Tectonic stage	Mineral and generation	Wm-bearing schists				Bt-bearing schists			
<b>White mica</b>									
		Si	Ti	X <sub>Mg</sub>	X <sub>Fe</sub>	N.D.	N.D.	N.D.	N.D.
Pre-S <sub>1</sub>	WmI	6.05–6.15; 6.11 ± 0.03	0.05–0.16; 0.09 ± 0.03	0.36–0.53; 0.45 ± 0.05	0.07–0.10; 0.08 ± 0.01	N.D.	N.D.	N.D.	N.D.
Syn-S <sub>1</sub>	WmII	6.05–6.16; 6.11 ± 0.03	0.05–0.16; 0.08 ± 0.02	0.38–0.66; 0.46 ± 0.06	0.06–0.10; 0.09 ± 0.01	N.D.	N.D.	N.D.	N.D.
Post-S <sub>1,b</sub>	WmIII	6.03–6.16; 6.10 ± 0.04	0.01–0.08; 0.06 ± 0.02	0.28–0.58; 0.46 ± 0.07	0.06–0.09; 0.08 ± 0.01	N.D.	N.D.	N.D.	N.D.
<b>Biotite</b>									
		Ti	Al <sup>IV</sup>	X <sub>Mg</sub>	N.D.	Ti	Al <sup>IV</sup>	X <sub>Mg</sub>	N.D.
Pre-S <sub>1</sub>	BtI	0.21–0.43; 0.32 ± 0.05	0.78–1.08; 0.91 ± 0.07	0.32–0.46; 0.38 ± 0.04	N.D.	0.31–0.44; 0.38 ± 0.04	0.46–0.59; 0.51 ± 0.05	0.37–0.47; 0.43 ± 0.04	N.D.
Syn-S <sub>1</sub>	BtII	0.08–0.39; 0.27 ± 0.08	0.82–1.12; 0.95 ± 0.08	0.34–0.49; 0.39 ± 0.04	N.D.	0.31–0.45; 0.38 ± 0.04	0.40–0.64; 0.53 ± 0.06	0.41–0.48; 0.45 ± 0.02	N.D.
Post-S <sub>1,a</sub>	BtIII	0.12–0.51; 0.29 ± 0.07	0.75–1.39; 0.95 ± 0.14	0.33–0.43; 0.39 ± 0.02	N.D.	0.23–0.43; 0.37 ± 0.06	0.48–0.68; 0.56 ± 0.07	0.42–0.46; 0.44 ± 0.01	N.D.
<b>Garnet</b>									
		Fe <sup>2+</sup>	Mn	Mg	Ca	Fe <sup>2+</sup>	Mn	Mg	Ca
Pre-S <sub>1</sub>	GrtI	2.08–2.33; 2.21 ± 0.08	0.15–0.39; 0.28 ± 0.07	0.31–0.42; 0.35 ± 0.03	0.10–0.20; 0.14 ± 0.02	1.81–1.97; 1.88 ± 0.07	0.15–0.35; 0.25 ± 0.07	0.15–0.28; 0.22 ± 0.05	0.59–0.64; 0.62 ± 0.02
Syn-S <sub>1</sub>	GrtII	2.09–2.36; 2.23 ± 0.08	0.13–0.42; 0.27 ± 0.06	0.29–0.45; 0.37 ± 0.04	0.08–0.15; 0.11 ± 0.02	1.79–2.06; 1.95 ± 0.07	0.15–0.31; 0.19 ± 0.04	0.27–0.39; 0.36 ± 0.04	0.34–0.83; 0.47 ± 0.07
<b>Plagioclase</b>									
		Ab	An	Or	N.D.	Ab	An	Or	N.D.
Pre-S <sub>1</sub>	PlI	0.67–0.80; 0.75 ± 0.04	0.19–0.33; 0.24 ± 0.05	0.00–0.02; 0.01 ± 0.01	N.D.	0.46–0.67; 0.54 ± 0.04	0.37–0.53; 0.45 ± 0.05	0.01–0.01; 0.01 ± 0.00	N.D.
Syn-S <sub>1</sub>	PlII	0.72–0.82; 0.78 ± 0.03	0.17–0.27; 0.21 ± 0.03	0.01–0.03; 0.01 ± 0.00	N.D.	0.49–0.63; 0.56 ± 0.04	0.36–0.51; 0.43 ± 0.04	0.01–0.01; 0.01 ± 0.00	N.D.
Post-S <sub>1,a</sub>	PlIII	N.D.	N.D.	N.D.	N.D.	0.52–0.57; 0.55 ± 0.02	0.42–0.47; 0.44 ± 0.02	0.01–0.01; 0.01 ± 0.00	N.D.
Post-S <sub>1,b</sub>	PlIV	0.91–0.97; 0.95 ± 0.02	0.08–0.02; 0.04 ± 0.02	0.00–0.04; 0.02 ± 0.01	N.D.	N.D.	N.D.	N.D.	N.D.
<b>K-feldspar</b>									
		Ab	An	Or	N.D.	Ab	An	Or	N.D.
Syn-S <sub>1</sub>	KfsII	N.D.	N.D.	N.D.	N.D.	0.02	0	0.98	N.D.
Post-S <sub>1,b</sub>	KfsIV	0.01–0.04; 0.03 ± 0.01	0.00–0.00; 0.00 ± 0.00	0.96–0.99; 0.97 ± 0.01	N.D.	N.D.	N.D.	N.D.	N.D.
<b>Chlorite</b>									
		Al	X <sub>Mg</sub>	N.D.	N.D.	Al	X <sub>Mg</sub>	N.D.	N.D.
Post-S <sub>1,b</sub>	Fractures of Grt	5.28–5.02; 5.69 ± 0.38	0.35–0.41; 0.39 ± 0.03	N.D.	N.D.	3.25–3.26; 3.26 ± 0.00	0.12–0.32; 0.22 ± 0.14	N.D.	N.D.
	after Bt	5.11–5.54; 5.34 ± 0.17	0.27–0.41; 0.36 ± 0.06	N.D.	N.D.	N.D.	N.D.	N.D.	N.D.
	shear zone	5.38–5.62; 5.51 ± 0.08	0.38–0.62; 0.46 ± 0.12	N.D.	N.D.	N.D.	N.D.	N.D.	N.D.
	after Wm	5.54	0.31	N.D.	N.D.	N.D.	N.D.	N.D.	N.D.

Note: Wm—white mica; Bt—biotite. Cations are expressed in atoms per formula unit (a.p.f.u.), whereas molar fractions and feldspar and members are normalized to one. The maximum and minimum values (first line of table boxes) and average with standard deviation (second line of the table box) are reported for each mineral generation. Samples of Wm-bearing schist are: 8, 13, 42, 52, and 55; samples of Bt-bearing schist are 44 and 46; see Figure 2 for sample locations. Mineral proportional formulae on the basis of: 22 oxygen atoms for biotite and white mica, 12 oxygen atoms for garnet, 8 oxygen atoms for feldspar, and 28 oxygen atoms for chlorite. Fe<sup>2+</sup> was recalculated for garnet only. Mineral abbreviations are according to Whitney and Evans (2010) with the exception of Wm (white mica).

TABLE 2. 1D-TIMS DATA

Faction size	Wt [μg]	U [ppm]	PbA [ppm]	mPb/mPbA	Pb [pg]	mPb [%]	ThU <sup>232</sup> [%]	mPb/mU [%]	mPb/mU [%]	mPb/mPb [%]	mPb/mU age [Ma]	Correlation coefficient	mPb/mPb age [Ma]	Discordance <sup>a</sup> [%]
Sample 122 Joes Mountain orthogneiss, UTM 266478E, 5630060N														
B (s, 149-252)	2	1229	61	190	43	7.8	0.29	0.05093 ± 0.72	0.3740 ± 2.8	0.05339 ± 2.2	319.5 ± 4.5	0.5936	345.4 ± 93.2	7.7
C (s, 149-252)	2	600	51	212	21	7.7	0.26	0.05586 ± 0.26	0.4126 ± 1.6	0.05075 ± 1.5	260.4 ± 1.8	0.6226	260.4 ± 66.7	2.9
E (st 105-149)	1	2250	125	267	26	9	0.33	0.05573 ± 0.46	0.4134 ± 1.1	0.05376 ± 0.6	346.6 ± 3.1	0.5606	362.4 ± 40.0	3.6
V (s, 935-149)	3	349	19	494	8	8.3	0.30	0.05549 ± 0.63	0.4129 ± 0.4	0.05419 ± 0.71	349.1 ± 3.2	0.5349	375.3 ± 32.1	7.4
J (s, 935-149)	3	249	14	398	7	7.8	0.29	0.05731 ± 0.33	0.4239 ± 0.7	0.05393 ± 0.3	359.2 ± 2.3	0.5472	355.5 ± 37.8	-1.07
K (st 105-149)	2	760	44	660	6	9	0.30	0.05581 ± 0.29	0.4124 ± 0.8	0.05379 ± 0.4	350.1 ± 2.0	0.5464	359.6 ± 18.0	2.7
Sample 4 Joes Mountain pegmatite, cross-cutting F <sub>2</sub> folds, UTM 267200E, 5625679N														
A (st 149-252)	50	4102	40	572	250	0.7	0.025	0.010711 ± 0.18	0.07067 ± 0.64	0.04769 ± 0.6	68.7 ± 0.3	0.5222	68.6 ± 26.7	30.5
B (st 149-252)	21	5700	57	210	430	1.4	0.046	0.010816 ± 0.25	0.07231 ± 1.7	0.04646 ± 1.5	69.4 ± 0.3	0.6411	122.7 ± 73.1	43.7
D (st 74-935)	25	671	7	1319	8	6.4	0.225	0.019367 ± 0.29	0.09993 ± 0.34	0.05014 ± 2.1	84.8 ± 0.4	0.7951	201.8 ± 9.7	89.3
M1 (s, 149-252)	26	25,430	424	6760	64	53.4	3.729	0.066815 ± 0.57	0.06664 ± 0.57	0.04611 ± 0.12	56.6 ± 0.6	0.9778	3.2 ± 5.8	-669
M2 (s, 149-252)	26	18,467	426	6665	50	56.5	4.225	0.011209 ± 0.78	0.07247 ± 0.78	0.04626 ± 0.12	72.7 ± 1.1	0.9879	16.1 ± 5.8	-263.9
M3 (s, 149-252)	59	12,736	277	6230	61	51.3	3.436	0.010667 ± 0.43	0.06592 ± 0.40	0.04616 ± 0.19	70.4 ± 0.6	0.9661	5.8 ± 9.3	-659
M4 (s, 149-252)	24	30,938	693	4932	935	54.9	3.993	0.019299 ± 0.24	0.07095 ± 0.25	0.04617 ± 0.09	71.2 ± 0.3	0.9707	8.4 ± 2.9	-933
M5 (s, 149-252)	12	50,833	1143	7945	59	53	3.715	0.011713 ± 0.29	0.07999 ± 0.38	0.04653 ± 0.20	75.1 ± 0.8	0.9879	173.0 ± 9.2	59.9

Note: 1D-TIMS—laser-ablation-thermal ionization-mass spectrometry. Errors are 1 std. error of mean in %, except for age errors, which are 2 std. errors in Ma.

<sup>a</sup>Discordance Pb.

<sup>b</sup>Single grain (s), multiple grains (m), single sp (sp), or multiple (st); shown in micrometers.

<sup>c</sup>Includes sample weight error of ±0.001 mg in concentration uncertainty.

<sup>d</sup>Total amount Pb in analysis.

<sup>e</sup>ThU from 2067506<sup>b</sup> and 2079206<sup>b</sup> age.

<sup>f</sup>Discordance on discord to origin.



TABLE 4. VARIATION OF CONDITIONS DURING DEVELOPMENT OF TECTONIC STAGES

Stage	Av P (GPa)	Av T (°C)	Av P/T (GPa/°C)	Av D (km)	Av T/D (°C/km)
<u>Wm-schist</u>					
Pre-S <sub>1</sub>	0.62	651	$0.95 \times 10^{-3}$	22	30
Syn-S <sub>1</sub>	0.61	641	$0.95 \times 10^{-3}$	21	30
Post-S <sub>1a</sub>	0.42	647	$0.65 \times 10^{-3}$	15	44
<u>Bt-schist</u>					
Pre-S <sub>1</sub>	0.88	671	$1.30 \times 10^{-3}$	31	22
Syn-S <sub>1</sub>	0.83	701	$1.18 \times 10^{-3}$	29	24
Post-S <sub>1a</sub>	0.40	665	$0.63 \times 10^{-3}$	15	45

Note: Average pressure (Av P), temperature (Av T), pressure/temperature ratio (Av P/T), depth (Av D), and temperature/depth ratio (Av T/D) for the successive deformation stages in Wm- and Bt-bearing schist. Wm—white mica; Bt—biotite. Pre-S<sub>1</sub> is the condition for the assemblage yielding the retrograde path. Depth is estimated taking into account an average density for the continental crust of 2.9 g/cm<sup>3</sup> (Spear, 1993).